by incubation in PBS-MT (PBS, 2% skim milk, 0.1% Triton X-100) for 30 min at room temperature, the cells were incubated with primary antibodies in PBS-MT for 1 h at room temperature, followed by incubation with secondary antibodies. The primary antibodies used were as follows: MyHC mouse monoclonal antibody (clone MF20, Hybridoma Bank) to detect differentiated cells, anti-GFP mouse monoclonal antibody (Invitrogen) to detect transfected cells, anti-phosphorylated histone H3 (phospho-HH3) rabbit polyclonal antibody (Upstate Biotechnology, Lake Placid, NY, USA) to detect mitotic nuclei, and anti-BrdU mouse monoclonal antibody (Zymed, South San Francisco, CA, USA) to detect DNA synthesis. The secondary antibodies were as follows: AlexaFluor488-conjugated anti-mouse IgG and AlexaFluor546-conjugated anti-rabbit IgG antibodies (Molecular Probes, Eugene, OR, USA). For a BrdU assay, cell cultures were maintained for 2.5 h with 1 μM of BrdU. 4′,6-Diamidino-2-phenylindole (DAPI) was used to see the nuclei (0.5 μg/mL).

Analysis of interactions between proteins and mRNAs

C2C12 cells were transfected with over-expression vectors expressing FLAG-tagged Rbm24, Rbm38 or mock for 5 h, then immunoprecipitation was carried out as previously described (Peritz *et al.* 2006). The antibody-antigen-RNA binding protein complexes were subjected to immunoprecipitation with protein G agarose beads, then DNase (Invitrogen) treatment was carried out completely before RNA extraction. Five percent of the cell extract was used directly for total RNA isolation, with the remaining portion incubated with Protein G agarose beads (Invitrogen) conjugated with monoclonal anti-Flag M2 (Sigma) or anti-IgG1 control antibody (BD Pharmingen, San Diego, CA, USA) for 4 h. Reverse transcription was carried out using Super Script III (Invitrogen). The sense primer, 5′-CCCTCTCCCAGTCTCCAAAC-3′ and antisense primer, 5′-TAAGGGCCCTACCGTCCTAC-3′, were designed to amplify the entire p21 ORF, which was carried out for 1 min at 94 °C, 30 s at 55 °C and 1 min at 72 °C for 35 cycles. The primers used to amplify the GAPDH transcripts were as follows: forward primer, 5′-TGAAGGTCGGAGTCAACGGATTTGGT-3′ and reverse primer, 5′-CATGTGGGCCATGAGGTCCACCAC-3′.

Acknowledgements

We express our thanks to the members of the Department of Bioscience for their technical support. This work was supported by a Grant-in-Aid for Scientific Research from the Ministry of Education, Culture, Sports, Science and Technology of Japan, and by grants from the Japan Science and Technology Corporation, the Ministry of Health, Labour and Welfare of Japan, and the Program for Promotion of Fundamental Studies in Health Sciences of the National Institute of Biomedical Innovation (NIBIO).

References

Anyanful, A., Ono, K., Johnsen, R.C., Ly, H., Jensen, V., Baillie, D.L. & Ono, S. (2004) The RNA-binding protein SUP-12 controls muscle-specific splicing of the ADF/cofilin pre-mRNA in *C. elegans*. *J. Cell Biol.* **167**, 639–647.

Bischoff, R. & Holtzer, H. (1969) Mitosis and the processes of differentiation of myogenic cells *in vitro*. *J. Cell Biol.* **41**, 188–200.

Brugarolas, J., Moberg, K., Boyd, S.D., Taya, Y., Jacks, T. & Lees, J.A. (1999) Inhibition of cyclin-dependent kinase 2 by p21 is necessary for retinoblastoma protein-mediated G1 arrest after gamma-irradiation. *Proc. Natl Acad. Sci. USA* **96**, 1002–1007.

Clegg, C.H., Linkhart, T.A., Olwin, B.B. & Hauschka, S.D. (1987) Growth factor control of skeletal muscle differentiation: commitment to terminal differentiation occurs in G1 phase and is repressed by fibroblast growth factor. *J. Cell Biol.* **105**, 949–956.

el-Deiry, W.S., Harper, J.W., O'Connor, P.M., *et al.* (1994) WAF1/CIP1 is induced in p53-mediated G1 arrest and apoptosis. *Cancer Res.* **54**, 1169–1174.

el-Deiry, W.S., Tokino, T., Velculescu, V.E., Levy, D.B., Parsons, R., Trent, J.M., Lin, D., Mercer, W.E., Kinzler, K.W. & Vogelstein, B. (1993) WAF1, a potential mediator of p53 tumor suppression. *Cell* **75**, 817–825.

Deng, C., Zhang, P., Harper, J.W., Elledge, S.J. & Leder, P. (1995) Mice lacking p21CIP1/WAF1 undergo normal development, but are defective in G1 checkpoint control. *Cell* **82**, 675–684.

Dreyfuss, G., Matunis, M.J., Pinol-Roma, S. & Burd, C.G. (1993) hnRNP proteins and the biogenesis of mRNA. *Annu. Rev. Biochem.* **62**, 289–321.

Figueroa, A., Cuadrado, A., Fan, J., Atasoy, U., Muscat, G.E., Muñoz-Canoves, P., Gorospe, M. & Muñoz, A. (2003) Role of HuR in skeletal myogenesis through coordinate regulation of muscle differentiation genes. *Mol. Cell. Biol.* **23**, 4991–5004.

Fukada, S., Uezumi, A., Ikemoto, M., Masuda, S., Segawa, M., Tanimura, N., Yamamoto, H., Miyagoe-Suzuki, Y. & Takeda, S. (2007) Molecular signature of quiescent satellite cells in adult skeletal muscle. *Stem Cells* **25**, 2448–2459.

Giles, K.M., Daly, J.M., Beveridge, D.J., Thomson, A.M., Voon, D.C., Furneaux, H.M., Jazayeri, J.A. & Leedman, P.J. (2003) The 3′-untranslated region of p21WAF1 mRNA is a composite cis-acting sequence bound by RNA-binding proteins from breast cancer cells, including HuR and poly(C)-binding protein. *J. Biol. Chem.* **278**, 2937–2946.

Guo, K., Wang, J., Andres, V., Smith, R.C. & Walsh, K. (1995) MyoD-induced expression of p21 inhibits cyclin-dependent kinase activity upon myocyte terminal differentiation. *Mol. Cell. Biol.* **15**, 3823–3829.

Halevy, O., Novitch, B.G., Spicer, D.B., Skapek, S.X., Rhee, J., Hannon, G.J., Beach, D. & Lassar, A.B. (1995) Correlation of terminal cell cycle arrest of skeletal muscle with induction of p21 by MyoD. *Science* **267**, 1018–1021.

Kablar, B., Krastel, K., Tajbakhsh, S. & Rudnicki, M.A. (2003) Myf5 and MyoD activation define independent myogenic compartments during embryonic development. *Dev. Biol.* **258**, 307–318.

Krecic, A.M. & Swanson, M.S. (1999) hnRNP complexes: composition, structure, and function. *Curr. Opin. Cell Biol.* **11**, 363–371.

Lu, J.Y. & Schneider, R.J. (2004) Tissue distribution of AU-rich mRNA-binding proteins involved in regulation of mRNA decay. *J. Biol. Chem.* **279**, 12974–12979.

Miller, R.A., Christoforou, N., Pevsner, J., McCallion, A.S. & Gearhart, J.D. (2008) Efficient array-based identification of novel cardiac genes through differentiation of mouse ESCs. *PLoS ONE* **3**, e2176.

Mochizuki, N., Yamashita, S., Kurokawa, K., Ohba, Y., Nagai, T., Miyawaki, A. & Matsuda, M. (2001) Spatio-temporal images of growth-factor-induced activation of Ras and Rap1. *Nature* **411**, 1065–1068.

Nadal-Ginard, B. (1978) Commitment, fusion and biochemical differentiation of a myogenic cell line in the absence of DNA synthesis. *Cell* **15**, 855–864.

Odelberg, S.J., Kollhoff, A. & Keating, M.T. (2000) Dedifferentiation of mammalian myotubes induced by msx1. *Cell* **103**, 1099–1109.

Peritz, T., Zeng, F., Kannanayakal, T.J., Kilk, K., Eiríksdóttir, E., Langel, U. & Eberwine, J. (2006) Immunoprecipitation of mRNA-protein complexes. *Nat. Protoc.* **1**, 577–580.

Shi, L., Zhao, G., Qiu, D., Godfrey, W.R., Vogel, H., Rando, T.A., Hu, H. & Kao, P.N. (2005) NF90 regulates cell cycle exit and terminal myogenic differentiation by direct binding to the 3′-untranslated region of MyoD and p21WAF1/CIP1 mRNAs. *J. Biol. Chem.* **280**, 18981–18989.

Shim, J., Lim, H., J, R.Y. & Karin, M. (2002) Nuclear export of NF90 is required for interleukin-2 mRNA stabilization. *Mol. Cell* **10**, 1331–1344.

Shu, L., Yan, W. & Chen, X. (2006) RNPC1, an RNA-binding protein and a target of the p53 family, is required for maintaining the stability of the basal and stress-induced p21 transcript. *Genes Dev.* **20**, 2961–2972.

Sorrentino, V., Pepperkok, R., Davis, R.L., Ansorge, W. & Philipson, L. (1990) Cell proliferation inhibited by MyoD1 independently of myogenic differentiation. *Nature* **345**, 813–815.

Terami, H., Hidaka, K., Shirai, M., Narumiya, H., Kuroyanagi, T., Arai, Y., Aburatani, H. & Morisaki, T. (2007) Efficient capture of cardiogenesis-associated genes expressed in ES cells. *Biochem. Biophys. Res. Commun.* **355**, 47–53.

Wang, W., Furneaux, H., Cheng, H., Caldwell, M.C., Hutter, D., Liu, Y., Holbrook, N. & Gorospe, M. (2000) HuR regulates p21 mRNA stabilization by UV light. *Mol. Cell. Biol.* **20**, 760–769.

Xiao, L., Rao, J.N., Zou, T., Liu, L., Marasa, B.S., Chen, J., Turner, D.J., Zhou, H., Gorospe, M. & Wang, J.Y. (2007) Polyamines regulate the stability of activating transcription factor-2 mRNA through RNA-binding protein HuR in intestinal epithelial cells. *Mol. Biol. Cell* **18**, 4579–4590.

Yamaguchi, A. (1995) Regulation of differentiation pathway of skeletal mesenchymal cells in cell lines by transforming growth factor-beta superfamily. *Semin. Cell Biol.* **6**, 165–173.

Yang, X., Wang, W., Fan, J., Lal, A., Yang, D., Cheng, H. & Gorospe, M. (2004) Prostaglandin A2-mediated stabilization of p21 mRNA through an ERK-dependent pathway requiring the RNA-binding protein HuR. *J. Biol. Chem.* **279**, 49298–49306.

Zhang, P., Wong, C., Liu, D., Finegold, M., Harper, J.W. & Elledge, S.J. (1999) $p21^{CIP1}$ and $p57^{KIP2}$ control muscle differentiation at the myogenin step. *Genes Dev.* **13**, 213–224.

Zhu, J., Jiang, J., Zhou, W. & Chen, X. (1998) The potential tumor suppressor p73 differentially regulates cellular p53 target genes. *Cancer Res.* **58**, 5061–5065.

Received: 16 December 2008
Accepted: 10 August 2009

T-box 2, a mediator of Bmp-Smad signaling, induced hyaluronan synthase 2 and Tgfβ2 expression and endocardial cushion formation

Manabu Shirai[a], Kyoko Imanaka-Yoshida[b], Michael D. Schneider[c], Robert J. Schwartz[d,1], and Takayuki Morisaki[e]

[a]Department of Bioscience, National Cardiovascular Center Research Institute, 5-7-1 Fujishirodai, Suita, Osaka 565-8565, Japan; [b]Department of Pathology and Matrix Biology, Mie University Graduate School of Medicine, 2-174 Edobashi, Tsu, Mie 514-8507, Japan; [c]Faculty of Medicine, National Heart and Lung Institute Imperial College London, London SW7 2AZ United Kingdom; [d]Institute of Biosciences and Technology, Texas A&M University System Health Science Center, 2121 West Holcombe Boulevard, Houston, TX 77030; and [e]Department of Molecular Pathophysiology, Osaka University Graduate School of Pharmaceutical Sciences, 1-6 Yamadaoka, Suita, Osaka 565-0871, Japan

Edited by Eric N. Olson, The University of Texas Southwestern Medical Center, Dallas, TX, and approved September 11, 2009 (received for review January 21, 2009)

During early heart development, Tbx2 gene expression is initiated in the cardiac crescent and then becomes restricted to the outflow tract and the atrioventricular region. We identified a *Tbx2* regulatory region, enriched in multiple Smad sites, sufficient to reproduce *Tbx2* expression patterns overlapping Bmp2 and Bmp4 gene activity in the heart. The role of *Tbx2* in cardiogenesis was analyzed by using Cre-LoxP activated *Tbx2* transgenic misexpression in chamber myocardium. Ventricular *Tbx2* misexpression exhibited an abnormally narrow chamber lumen owing to the expansion of *Hyaluronan synthase 2* expression in the ECM or cardiac jelly and the appearance of the endocardial cushions (ECs). Excessive *Tbx2* also induced *Tgfβ2*, which coincided with the outgrowth epithelial-mesenchymal transformed cells in ventricular and atrial tissues modifying cardiomyocyte identity from chamber type to non-chamber type. *Tbx2*, a central intermediary of Bmp-Smad signaling, has a central part in directing *Has2* and *Tgfβ2* expression, facilitating EC formation.

cardiac jelly | cardiomyocyte identity | epithelial-mesenchymal transformation | extracellular matrix | misexpression

The heart develops, as a modular organ, driven by distinct transcriptional regulatory programs that control each anatomical region (1). A member of the T-box factor family, *Tbx2*, which first appears in the cardiac crescent and then later restricted to non-chamber myocardium (My) [outflow tract (OFT), atrioventricular canal (AVC), inner curvature, and inflow tract) (2, 3)], is a valuable model of modular cardiac gene activity. *Tbx2* is central for endocardial cushion (EC) formation and chamber specification, and may be a transcriptional repressor (4, 5). Expression of chamber-specific myocardial genes, which include *Nppa* (encoding atrial natriuretic factor, *ANF*), *Gja5* (encoding connexin 40, *Cx40*), and *Gja1* (encoding connexin 43, *Cx43*), were repressed by *Tbx2* (3–5). *Tbx2* null mutant embryos exhibited small AVC and defective OFT septation (3), whereas *Tbx2* transgenic expression blocked chamber formation (4) and cell proliferation in the OFT and AVC (6).

The ECs form from localized expansion of the ECM also named cardiac jelly (7, 8) found in the cardiac OFT and AVC segments the simple heart tube into a complicated structure composed of the aortic sac, common ventricular chamber, and atrial chamber. Some endocardial cells invade into the ECM through epithelial-mesenchymal transformation (EMT) to remodel the cushion tissue into the mature valves. Several signaling pathways have been implicated in EC formation. The Bmp pathway is essential for both processes; expansion of ECM and EMT in the EC formation (9–14). Tgfβ2 performs crucial and sequential roles in EC formation and may also be regulated by Bmp2/4 during cardiogenesis (9–11). The hyaluronan (HA) synthase 2 (*Has2*) has been recently shown to have essential role in expansion of ECM and EMT (16). Also, *Tbx2* may be a direct target of Bmp2/4 signaling pathway during EC formation (2).

Here, we delineated an 80-bp regulatory region within the *Tbx2* 5′ flanking sequences, which contain multiple Smad DNA binding sites that recapitulate expression of *Tbx2* in the AVC and OFT. Previously, myocardial-specific inactivation of *Bmp2* also inhibited the appearance of several factors, including *Tbx2*, *Tgfβ2*, and *Has2*, and blocked cushion formation (9). To define the regulatory hierarchy shared by Bmp2/4-dependent genes, we analyzed embryos in which murine *Tbx2* was misexpressed in the developing chamber My, using a mouse genetic system based on Cre/loxP recombination. *Tbx2* altered cardiogenic lineage specification by expanding the ECM and EMT to drive EC formation via the induction of Tgfβ2 and Has2 gene activity in embryonic hearts.

Results

Smad Signaling Drives *Tbx2* Transgene Activity via a Distal Enhancer. *Tbx2* expression was first detected in the cardiac crescent and notochordal plate (Fig. 1*A*). At E8.5, *Tbx2* expression was maintained only in the posterior portion of the looping heart (Fig. 1*B*). As the heart matured, the expression of *Tbx2* became further limited to the AVC and OFT region (Fig. 1 *E* and *F*). *Tbx2* mRNA was also detected in the optic cups, otic vesicles, pharyngeal arches, and limb buds of embryonic day (E)9.5 and E10.5 mouse embryos (Fig. 1 *C* and *D*). Transient F_0 transgenic mice harboring 4.1 kilobase (kb) of Tbx2 5′ flanking sequences linked to the *lacZ* reporter gene (Fig. 1*K*) revealed β-galactosidase activity in the OFT, AVC, and a portion of the left atrium, whereas LacZ activity was absent from the right atrium and the ventricles (Fig. 1*L*). Also, *Tbx2*, a downstream target of murine Bmp2/4 signaling (2, 9), was colocalized to the AVC and OFT (Fig. 1 *G–J*). After serial and gap deletion mutagenesis strategy, recapitulated *Tbx2* expression was delineated to a region between −3.4 and −2.6 kb in transgenic mouse embryos (Fig. 1 *L–O*).

Paired Smad 1/4 proteins, primary intracellular mediators of Bmp signals (12), activated transcription of the −4.1-kb reporter construct (Fig. 2*A*). Other Smad factor combinations did not strongly activate the *Tbx2* reporter, whereas the inhibitory Smad 6 (13, 14) blocked Tbx2 gene activity. *Tbx2* regulatory region

Author contributions: M.S., K.I.-Y., M.D.S., R.J.S., and T.M. designed research; M.S. performed research; M.D.S. contributed new reagents/analytic tools; M.S., K.I.-Y., R.J.S., and T.M. analyzed data; and M.S., K.I.-Y., R.J.S., and T.M. wrote the paper.

The authors declare no conflict of interest.

This article is a PNAS Direct Submission.

[1]To whom correspondence should be addressed. E-mail: rschwartz@ibt.tamhsc.edu.

This article contains supporting information online at www.pnas.org/cgi/content/full/0900635106/DCSupplemental.

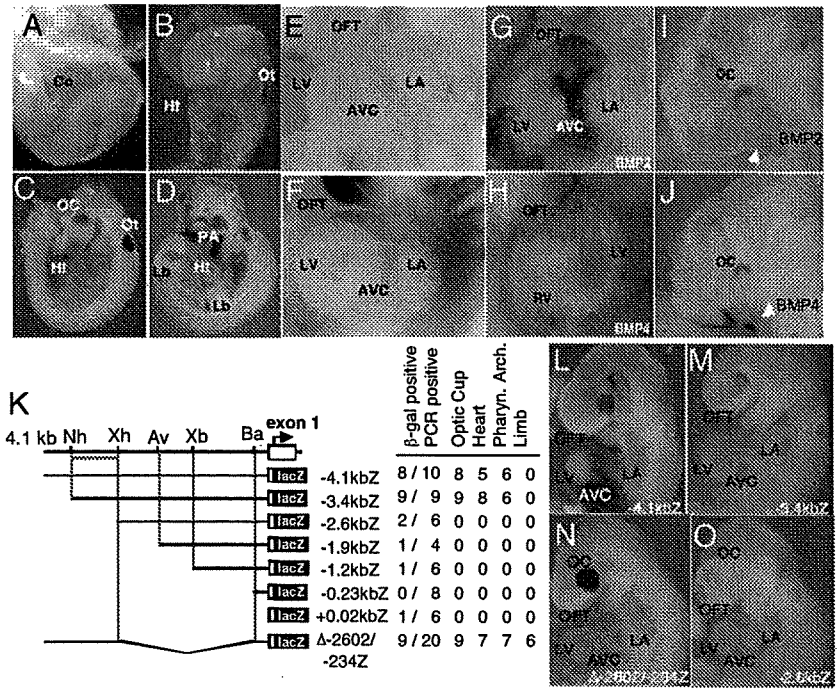

Fig. 1. Mouse Tbx2 gene activity in early cardiac development was recapitulated by distal *cis*-acting regulatory regions coincided with *Bmp2* and *Bmp4* expression. *Tbx2* expression was first detected in the cardiac crescent at E7.5 (*A*), and restricted to the posterior part of looping heart at E8.5 (*B*). The expression of *Tbx2* was also observed in the developing eye, otic cup, pharyngeal arches, and limb buds (*B*–*D*) At E9.5 and E10.5, *Tbx2* transcripts were localized in the OFT and AVC (*E* and *F*).. Expression of *Bmp2* and *Bmp4* (*G* and *H*) was observed in the OFT and AVC (*I* and *J*). Schematic representation of serial deleted 5′ flanking sequences of the Tbx2 gene, which were analyzed for transgene expression patterns in E9.5–E10.5 F_0 founder embryos (*K*). An upstream regulatory region that directs Tbx2 gene expression was indicated by a red bar. *LacZ* was expressed in the optic cup, heart, and pharyngeal arches using 4.1 kb (*L*), 3.4 kb (*M*), and Δ−2602/−234 (*N*) 5′ flanking fragments. No LacZ staining was observed in −2.6-kbZ transgenic embryos (*O*). Cc, cardiac crescent; Ht, heart; LA, left atrium; Lb, limb bud; LV, left ventricle; OC, optic cup; Ot, otic cup; PA, pharyngeal arch. Restriction sites shown above are: Nh, NheI; Xh, XhoI; Av, AvrII; Xb, XbaI; and Ba, BamHI.

responsive to Bmp signaling was localized to a 290-bp region expression in the developing heart (Fig. 2 *B* and *C*), which contains at least five conserved Smad sites, two of which, SBE1 and SBE5 sequences, were potent Smad1/4 cofactor binding sites (Fig. S1). Schematic representation of *Tbx2* transgenes analyzed in E9.5 F_0 embryos and a summary of the tissue restricted expression activity is shown in Fig. 2*C*, whereas five SMAD sites in SBE1-5 were mutated by site directed mutagenesis as shown in mSBE1-5 (Fig. 2*D*). The gap deletion mutant Δ−2899/−2602 hsp68lacZ construction, in which the five Smad sites were removed from the *Tbx2* 5′ flanking sequence, showed a complete loss of *lacZ* expression activity in the hearts of F_0 transgenic embryos (Fig. 2 *C* and *F*). The Smad site enriched region (SBE; −2916/−2602) linked to a minimal *hsp68* promoter *lacZ* transgene, revealed robust expression in the OFT and AVC, sufficient to recapitulate the restricted *Tbx2* expression pattern in the heart (Fig. 2 *C* and *G*), whereas site directed Smad site mutations eliminated gene activity in transgenic mice (Fig. 2 *C* and *H*).

Abnormal Deposition of ECM in *mTbx2*-Misexpressing Embryonic Hearts. To study the role of *Tbx2* in the cardiac morphogenesis, we generated transgenic mice that conditionally misexpressed murine Tbx2 gene in embryonic chamber-cardiomyocytes (Fig. 3 *A* and *B*; Fig. S2). Activated *Tbx2* embryos exhibited enlarged hearts, with marked myocardial hypoplasia associated with rich deposition of ECM in the compact and trabecular My (Fig. 3 *C* and *D*). Expansion of the EC (cardiac jelly) between the endocardium (En) and My (Fig. 3*E*) stained with alcian blue for acidic glycosaminoglycans (15) caused a narrow ventricular lumen. In control littermates, acidic glycosaminoglycans were deposited mainly in the ECM of OFT and AVC regions at E10.5 compared with the expanded ECM induced by activated *Tbx2*.

Glycosaminoglycan HA, a major constituent of the cardiac jelly, may be required for the expansion of EC (16,17). Excessive acidic glycosaminoglycans deposited through the cardiac tube in *mTbx2*-misexpressing embryos were also revealed by deposition of HA with the biotinylated-HA binding protein (BP; Fig. 3*F*). The specific binding of HABP to HA was eliminated by hyaluronidase treatment (Fig. S3). HA deposition was observed between the En and My in the inner curvature and the AVC of both control littermates and *mTbx2*-misexpressed mice, and in between the En and My of the outer curvature of *mTbx2*-misexpressed ventricles (Fig. 3*F*). Also, cultured cardiomyocytes from quartered hearts identified by *lacZ* and or by *Myh6* induced *mTbx2* expression (Fig. 3*G*; Fig. S4) were classified by the amount of HA secretion (Fig. 3*H*). *Tbx2*-misexpressing ventricular myocytes secreted greater amount of HA compared with ventricular myocytes from control littermates.

***Has2* and *Tgfβ2* are *Tbx2* Downstream Gene Targets.** Is there a hierarchical relationship between *Tbx2*, *Has2*, and *Tgfβ2*? HA synthatase (Has)2, the major enzyme responsible for HA synthesis in the AVC and atria, was strongly up-regulated in the ventricular My by *mTbx2* misexpression (Fig. 4). In comparison, other components of the ECM, including *Col1a1* (encoding type I collagen), *Cspg2* (encoding chondroitin sulfate proteoglycan 2, *versican*), *Fn1* (encoding fibronectin 1), and *Tnc* (encoding tenascin C) did not show obvious differences (data not shown). *Has2* is a direct Tbx2 target, because T-box binding sites were conserved between *Has2* promoter regions, which recruited en-

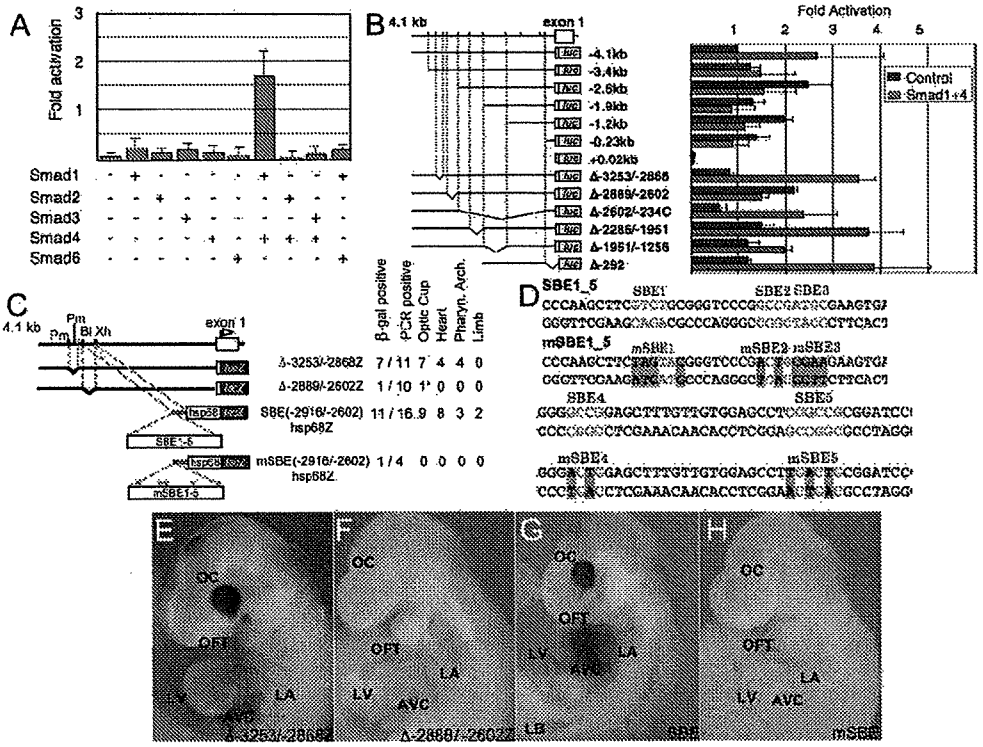

Fig. 2. Delineation of the distal Smad factor dependent *Tbx2* enhancer. (*A*) Multiple Smad expression vectors tranfected into CV1 cells revealed activation caused by Smad1/4 of the 4.1 kb of 5′ flanking sequence of *Tbx2* fused in-frame to the luciferase. The bars represent the average of three independent transfections, and the error bars represent the SE of corrected luciferase activity relative to the pCMV5 control vector. (*B*) Activation by Smad1/4 required the −2889/−2602 region. (*C*) Schematic representation of *Tbx2* transgenes analyzed in E9.5 F_0 embryos and a summary of the tissue restricted expression activity. (*D*) Five SMAD sites in SBE1-5 were mutated by site directed mutagenesis in mSBE1-5. (*E–J*) *LacZ* expression patterns in E9.5 F_0 embryos. (*E*) Δ−3253/−28682hsp68Z transgene; a gap deletion mutant, of a region immediately upstream of the multiSmad sites. (*F*) Δ−2899/−2602hsp68lacZ; a gap deletion mutant in which the multiple Smad sites were removed from the 5′ flanking sequence. (*G*) SBE(−2916/−2602)hsp68lacZ; the region from −2916 to −2602bp, containing five Smad sites, was linked to the hsp68lacZ reporter gene. (*H*) mSBE(−2916/−2602)hsp68lacZ; mutations were inserted at the multiple Smad sites in the −2916/−2602 fragment. *LacZ* expression were recapitulated by the DNA fragments containing Smad binding sites (*E* and *G*), whereas gap deletion and point mutagenesis of Smad binding sites eliminated gene activity in transgenic mice (*F* and *H*). Restriction sites are: *Bl*pI; Xh, XhoI.

dogenous Tbx2 from cardiac nuclear chromatin extracts and was transactivated by *Tbx2* (*SI Materials and Methods* and Fig. S5).

Tgfβ2 is normally expressed in the myocardial cells in the OFT and AVC, but was induced by *Myh6-Cre* activated *mTbx2* in ventricular and atrial My (Fig. 5 *A* and *B*). Also, phosphorylated Smad2 appeared in the endocardial and myocardial cells of *mTbx2*-activated ventricles and atria (Fig. 5*C*), which coincided with robust in vitro EMT assays (Fig. 5 *D* and *E*); thus, suggesting that the Tgfβ2 signaling pathway was activated by *mTbx2*. *Tgfβ2* may also be a direct target of Tbx2, because the *Tgfβ2* promoter has conserved T-box binding sites, bound endogenous Tbx2, and was activated with a *Tbx2*-expression vector (*SI Materials and Methods* and Fig. S6).

Discussion

Smad Factor Signaling Directed *Tbx2* Expression Through a Distal Enhancer During Early Murine Cardiogenesis. *Tbx2* transcripts first appear in the cardiac crescent and then later became restricted to the OFT and AVC during early avian (2) and mouse embryogenesis (Fig. 1). *Tbx2* is also expressed in the embryonic limb, optic cup, otic cup, and pharyngeal arches. Approximately 4 kb of 5′ flanking sequence of the murine Tbx2 gene was sufficient to reproduce much of these mouse embryonic expression patterns, as a *lacZ* reporter transgene. *LacZ* expression patterns closely overlapped with those of *Bmp2* and *Bmp4* in the heart and eye, and was delineated within the *Tbx2* 5′ flanking sequences, which contained Bmp directed multiple high-affinity binding sites for Smad transcription factors. Removal of these multiple Smad sites by gap deletion mutagenesis from the 4-kb flanking sequences blocked reporter gene activity in early embryos. In contrast, this short enhancer region linked to a minimal *hsp68* promoter was sufficient for steering the restricted expression of *lacZ* in a pattern, highly similar to the endogenous Tbx2 gene activity. Previously, application of Bmp2 selectively induced *cTbx2* expression in noncardiogenic embryonic tissue, and the Bmp antagonist Noggin down-regulated *cTbx2* activity (2). Also, the appearance of murine *Tbx2* was blocked in *Bmp2* null mouse embryos (2). Thus, *Tbx2* expression depended on Bmp signaling through Smad factors, a regulatory paradigm that also guides other modular-restricted genes in the developing heart.

***Tbx2* Directs EC Formation.** *Tbx2* is generally considered to be a transcriptional repressor. For example, *Tbx2*-null embryos have expanded chamber-specific gene expression into the AVC My (3). Also, *Tbx2*-overexpressing transgenic mice and *Tbx20*-null mice, in which *Tbx2* is up-regulated, exhibited decreased expression of several chamber-specific genes and caused hypoplasia of ventricular chamber (4–6, 18, 19). However, *Tbx2* also contains an activation domain (20), and is important for EC formation, because *Tbx2* null mutant embryos exhibited small AVC and defective OFT septation (3). As shown here, *Tbx2* enhanced ECM synthesis from myocardial cells and EMT from endocardial cells. Tbx2 directly bound *Has2* and *Tgfβ2* promoters and increased their transcriptional activities. Tgfβ signaling is crucial

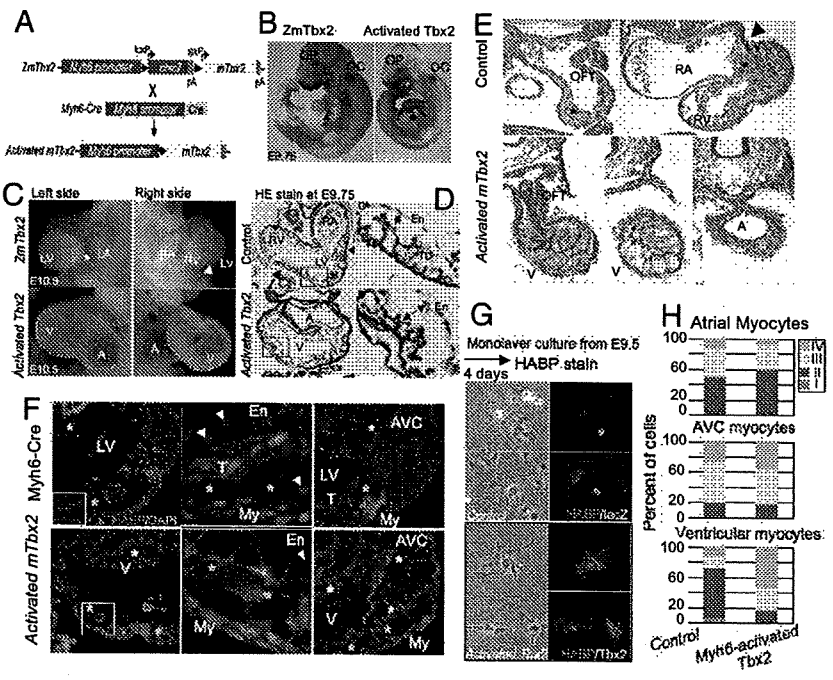

Fig. 3. Abnormal cardiac morphogenesis induced by activated *mTbx2* coincided with excessive HA deposition. (*A*) Schematic representation of *Myh6-Cre* induced activation of *mTbx2* by breeding *ZmTbx2* mice to the Cre deleter mouse line, *Myh6-Cre*. (*B*) Cardiomyocyte-specific activated *mTbx2* was detected by immunoperoxidase staining in the atria and ventricles at E9.75. (*C*) Enlarged images highlight embryonic hearts at E10.5. Relative to control littermates, activated *Tbx2* embryos exhibited an enlarged heart, which appeared as swollen single ventricular and atrial chambers, and a dilated AVC (yellow dotted line in *C*) at E10.5. (*D*) Histological sections of activated *mTbx2* in embryonic hearts at E9.75 stained with HE staining showed rounded ventricular chamber (blue dotted line) and an abnormally narrow ventricular lumen due to expansion of EC like structure between the En and My (two-headed arrow in *D*), and arrow indicate intraventricular sulcus (IVS) and arrowheads indicate AVC. (*E*) Histological sections of embryonic hearts stained at E10.5 with alcian blue revealed acidic glycosaminoglycans (blue stain) not only deposited in the OFT and AVC regions of control littermates (black asterisks), but throughout the chambers of activated *Tbx2* hearts (red asterisks). (*F*) Visualization of HA on sections of E9.75 embryos with HABP (red). HA was deposited between En and My in the inner curvature and AVC of activated *mTbx2* embryos and control littermates (white asterisks) and not in the outer curvature of control littermates. Extra deposition of HA was observed between En and My in the outer curvature of *mTbx2*-misexpressing ventricles (yellow asterisks). DAPI stain was used to visualize nuclei (blue). (*G*) Visualization of HA on cultured ventricular myocytes from embryos of E9.5 or E9.75 with HABP (red). Immunocytochemical detection of lacZ and Tbx2 (green). (*H*) Percentage of classified cardiomyocytes with HA secretion. Type I cardiomyocytes, no secretion of HA; Type II, little amount of HA around the cells; Type III, much HA is secreted around the cells; Type IV, much HA is secreted around the cells and deposited in the cells (Fig. S4). Majority of ventricular cardiomyocytes secreted excessive HA in the activated *mTbx2* embryos. T, trabeculae; CL, compact layer; and TL, trabecular layer.

for EMT in the AV cushions (20–22). Accelerated appearance of EMT from the ventricular and atrial tissues, in vitro EMT assays and increased Smad2 phosphorylation in *mTbx2*-activated embryos supports activation of Tgfβ2 pathway by Tbx2.

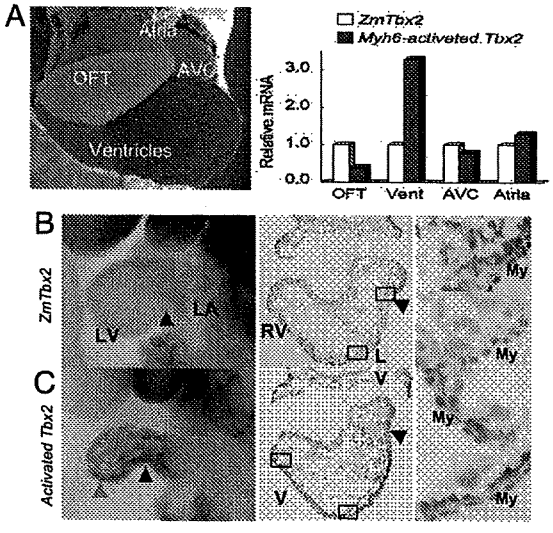

Fig. 4. HA synthetase, *Has2*, activated by *Tbx2* in cardiac chamber myocytes. (*A*) Real-time PCR analysis of dissected embryonic hearts at E9.5 or E9.75. *Has2* transcripts were tripled in the ventricles of activated *mTbx2* embryos. (*B*) Whole-mount in situ hybridization analysis for *Has2* expression was detected in the AVC (black arrowheads) of control littermates whereas expanded to ventricles (red arrowheads) of activated *Tbx2* embryos. The middle and right columns show sections after WISH. *Has2* expression was activated in ventricular myocardial cells of activated *Tbx2* embryos (right column). Nuclear were stained by nuclear fast red.

Tbx2 also induced *Has2* myocardial expression and increased HA deposition. HA is known as an essential factor for EC formation (8, 16, 23), and interacts with other molecules such as versican and fibrillin, which expands cardiac jelly providing extracellular space for cell migration (8). In addition to organizing extracellular environment, HA stimulates EMT of several types of epithelial cells (24) and endocardial cells dependent on Ras-activation (15) via ErbB2 receptor (23). In *Tbx2*-misexpressing embryos, extradeposition of HA was observed in the dilated chamber My; thus, *Tbx2* has an important role in EC formation by increasing synthesis of HA. During normal heart development, chamber-cardiomyocytes undergo a critical maturation step that is manifested by a transition from production to degradation of ECM between E8.0 and E9.5 (25). Whereas HA is required for cushion formation, excess HA deposition may cause hemodynamic alteration and prevent cardiomyocyte differentiation necessary for chamber maturation.

Hierarchical Relationship Between Bmp2/4, *Tbx2*, *Has2*, and *TGFβ2*. We propose a model in which Bmp-Smad responsive *Tbx2* is stimulated to perform a central role in promoting EC formation by inducing expansion of ECM and EMT by directing Has2 and Tgfβ2 gene activity (Fig. 6). Several signaling pathways have been implicated in EC formation. The Bmp pathway is essential for expansion of ECM and EMT in EC formation. Myocardial-specific inactivation of *Bmp2*, *Bmp4*, and a Bmp type I receptor gene, *Alk3*, respectively, failed to form the EC (9, 10, 26). Sugi et al. (11) demonstrated that Bmp2 could substitute for the My to induce EMT. Also, noggin treatment of explants efficiently inhibited EMT. In both chicken and mouse EMT assays, Tgfβ2 is able to replace the overlying My to activate EMT in *Tgfβ2* null mice (11, 16, 21, 22). Analysis of *Tgfβ2*-deficient mice also indicated that Tgfβ2 is important for valvulogenesis (27). Recent studies have shown that several factors, including *Tbx2*, *Tgfβ2*, and *Has2*, are downstream targets of Bmp2/4 pathway (9, 10). In

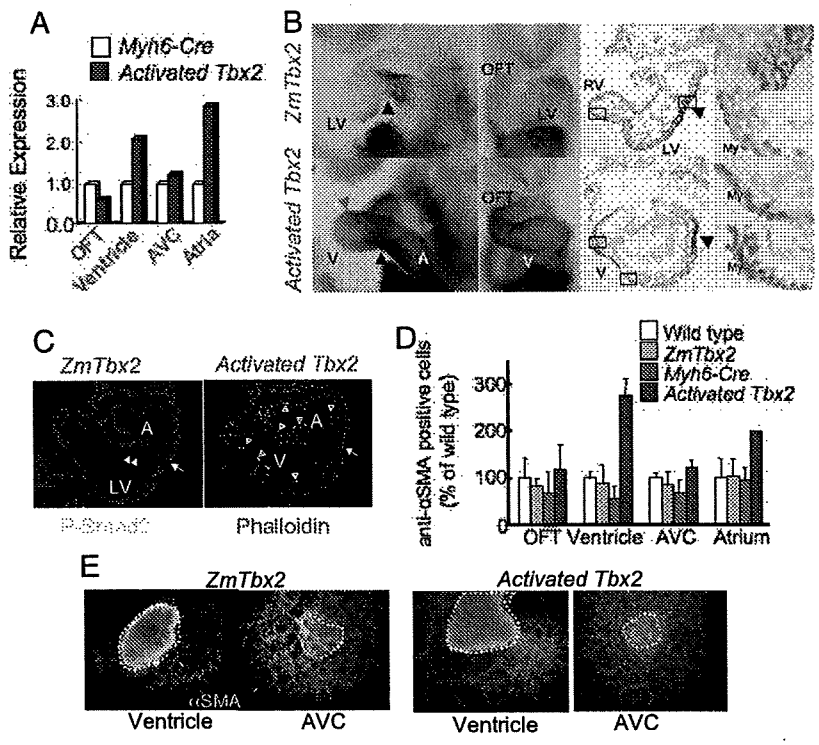

Fig. 5. Activated *mTbx2* induced *Tgfβ2* and enhanced EMT. (*A*) Real-time PCR analysis of quartered embryonic hearts at E9.5. *Tgfβ2* was increased in the ventricles and atria of activated *mTbx2* heart. (*B*) Whole-mount in situ hybridization analysis detected *Tgfβ2* expression in the AVC (black arrowheads in controls) and OFT of control littermates which expanded to ventricles and atria of activated *Tbx2* hearts (red arrowheads in misexpressed *Tbx2*). The middle and right columns show sections after WISH. *Tgfβ2* expression was activated in ventricular myocardial cells of activated *Tbx2* embryos (right column). Nuclear were stained by nuclear fast red. (*C*) Immunohistochemical detection of phospho-Smad2, an effector of Tgfβ signaling in the AVC (white arrows) En of control littermates (white arrowheads), which was expanded to the En of the ventricles and atria in activated *mTbx2* hearts (red arrowheads). (*D* and *E*) Immunohistochemical detection of α-smooth muscle actin (SMA) showed increased EMT in in vitro collagen gel assays of ventricular and atrial explants. The percentage of anti-αSMA positive cells formed in explants from *mTbx2*-misexpressing ventricles and atria was approximately doubled compared with controls.

addition to myocardial-derived Bmp function, Bmp signals directly to the cushion En through the Bmpr1a to induce EMT (9). In our experiments, Bmp2/4 were not up-regulated in *Tbx2*-misexpressing embryos (Fig. S7). Recently, Singh et al. (28) showed that Tbx20 directly interfered with Bmp/Smad signaling to suppress Tbx2 expression in the chambers; thereby, confining Tbx2 expression to the prospective AVC region. They also confirmed our observation that Tbx2 distal enhancer directs Tbx2 expression to the AVC and OFT. Here, we showed Bmp-Smad signaling dependent *Tbx2* expression directed *Has2* and *Tgfβ2* gene activity to coordinately regulate EC formation.

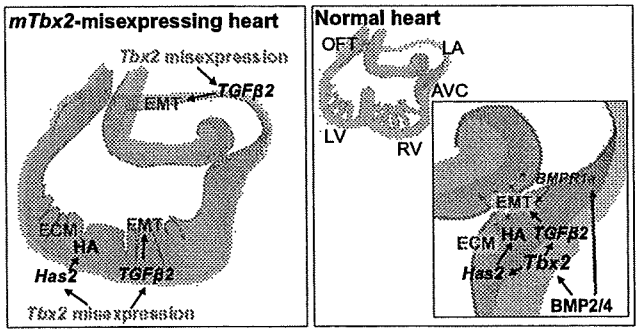

Fig. 6. Model of *Tbx2* function for the EC formation in the AVC. The *mTbx2* misexpression induces expression of *Has2*; thereby, driving the synthesis and deposition of HA and/or cardiac jelly through the heart. Misexpressed *Tbx2* signals also promoted expression of Tgfβ2 gene that supports the induction of EMT in the ventricles and atria. In the normal heart development, *Tbx2* works as one of the important factor to induce expansion of ECM and EMT under the Bmp2/4-Smad signaling pathway. Bmp signals also directly to the En through the Bmpr1a.

Experimental Procedures

Generation of *mTbx2* Reporter Gene Constructions. A genomic fragment that contained the *Tbx2* locus was isolated from a 129SVJ mouse genomic library. A 4.5-kb NotI fragment flanking the 5′ transcription start site and overlapping the first coding exon was cloned into the NotI site of pBluescript-KS for sequencing. The *mTbx2* reporter construct were generated from 4.1 kb of *mTbx2* flanking sequence 5′ was linked in-frame in front of the *lacZ* and luciferase cDNA from pPD46.21 and pGL3-Basic (Promega). Deletion constructs were generated by restriction endonuclease digestion. The region from −2916 to −2602bp, containing multiple Smad sites, was linked to the hsp68lacZ reporter gene (29). Mutations at multiple Smad sites in −2916/−2602 fragment were inserted using In-Fusion PCR cloning kit (Clontech) (Fig. 2*D*; Fig. S1*C*).

Whole-Mount in Situ Hybridization. Staged mouse embryos were obtained after timed mating of mice with the morning of the copulation plug being E0.5. Embryos were fixed in MEMFA (0.1 M Mops/2 mM EGTA/1 mM $MgSO_4$/3.7% formaldehyde) and stored in 90% methanol at −20 °C until use for hybridization. Whole-mount in situ hybridization was performed as described by Yamada et al. (2), except that polyvinyl alcohol was included to increase signal intensity. A full-length of *mTbx2* cDNA (kindly provided by Roni Bollag) was cloned into the *EcoR*I site of pBluescript-KS to synthesize digoxigenin-labeled RNA probes. After restriction endonuclease digestion with SacI, antisense probes were transcribed with RNA labeling kit (Stratagene).

Transient Transfection Assays. Monkey CV-1 fibroblasts were grown in DMEM with 10% FBS. Cells were plated at 1×10^5 cells per well in a 24-well plate and transfected 24 h later with DNA mixture containing a total of 2 μg of total DNA, which included 500 ng of luciferase reporter vector, 500 ng of β-galactosidase vector, and a total of 1 μg of pCMV5-derived vectors. Transfections were performed using Lipofectamine (Invitrogen) as described (30). Luciferase activity were measured using a luminometer to detect activates substrates, then normalized by β-galactosidase activity (29).

Histology. Embryos were dissected in Dulbeco's PBS and fixed overnight at 4 °C in 4% PFA in PBS for histological analysis. After fixation, embryos were rinsed in PBS, then dehydrated through graded ethanol or methanol and embedded in paraffin wax. Sections were cut and stained with hematoxylin-eosin or alcian blue according to standard methods. The HA was detected with 2 μg/mL biotinylated HABP isolated from bovine nasal cartilage (Seikagaku). The HABP was detected using streptavidin-conjugated AlexaFluor (Invitrogen). For immunohistochemistry, sections were incubated with rabbit anti-TBX2 IgG (Upstate Biotechnology) or rabbit anti-β-galactosidase (Biogenesis). Primary antibody was detected with goat anti-rabbit IgG labeled with Alexa Fluor (Invitrogen).

Real-Time PCR. Embryonic hearts at E9.5–E9.75 were divided to 4-parts, OFT, ventricles, AVC, atria at the posterior boundary of EC in OFT, anterior and posterior boundaries of EC. Dissected tissues were immediately frozen in liquid nitrogen and stored at −80 °C until embryo and yolk sac DNA was genotyped. Total RNA isolation and first strand cDNA synthesis were performed with TRIzol reagent, SuperScript III (Invitrogen) and random primer, as per the manufacturer's instructions.

Primary Culture of Embryonic Cardiac Cells and Classification of Cardiomyocytes with HA Synthesis. Quartered embryonic cardiac tissues were separated as described above. After trypsinization, isolated cardiac cells were cultured on gelatinized dishes by using culture medium containing DMEM (D5796; Sigma–Aldrich), 10% heat-inactivated FCS (HyClone), 0.1 g/mL penicillin, and 0.1 mg/mL streptomycin. After 4 days culture, cells were fixed in 4% PFA in PBS and detected HA, Tbx2 and β-galactosidase as described above. Classification of cardiomyocytes with HA secretion was followed as described in Fig. S4.

1. Schwartz RJ, Olson EN (1999) Building the heart piece by piece: Modularity of *cis*-elements regulating to Nkx2–5 transcription. *Development* 126:4187–4192.
2. Yamada M, et al. (2000) Expression Of Chick Tbx-2, Tbx-3 and Tbx-5 genes during early heart development: Evidence for BMP2 induction of Tbx2. *Dev Biol* 228:95–105.
3. Harrelson Z, et al. (2004) Tbx2 is essential for patterning the atrioventricular canal and for morphogenesis of the outflow tract during heart development. *Development* 131:5041–5052.
4. Christoffels VM, et al. (2004) T-box transcription factor Tbx2 represses differentiation and formation of the cardiac chambers. *Devl Dyn* 229:763–770.
5. Habets PE, et al. (2002) Cooperative action of Tbx2 and Nkx2.5 inhibits ANF expression in the atrioventricular canal: Implications for cardiac chamber formation. *Genes Dev* 16:1234–1246.
6. Cai CL, et al. (2005) T-box genes coordinate regional rates of proliferation and regional specification during cardiogenesis. *Development* 132:2475–2487.
7. Pierpont ME, Markwald RR, Lin AE (2001) Genetic aspects of atrioventricular septal defects. *Am J Med Genet* 297:289–296.
8. Schroeder JA, Jackson LF, Lee DC, Camenisch TD (2003) Form and function of developing heart valves: Coordination by extracellular matrix and growth factor signaling. *J Mol Med* 81:392–403.
9. Ma L, Lu MF, Schwartz RJ, Martin JF (2005) Bmp2 is essential for cardiac cushion epithelial-mesenchymal transition and myocardial patterning. *Development* 132:5601–5611.
10. Gaussin V, et al. (2002) Endocardial cushion and myocardial defects after cardiac myocyte-specific conditional deletion of the bone morphogenetic protein receptor ALK3. *Proc Natl Acad Sci USA* 99:2878–2883.
11. Sugi Y, Yamamura H, Okagawa H, Markwald RR (2004) Bone morphogenetic protein-2 can mediate myocardial regulation of atrioventricular cushion mesenchymal cell formation in mice. *Dev Biol* 269:505–518.
12. Itoh S, Itoh F, Goumans MJ, Ten Dijke P (2000) Signaling of transforming growth factor-beta family members through Smad proteins. *Eur J Biochem* 267:6954–6967.
13. Galvin KM, et al. (2000) A role for smad6 in development and homeostasis of the cardiovascular system. *Nat Genet* 24:171–174.
14. Yamada M, et al. (1999) Evidence for a role of Smad6 in chick cardiac development. *Dev Biol* 215:48–61.
15. Whiteman P (1973) The quantitative measurement of Alcian Blue glycosaminoglycan complexes. *Biochem J* 131:343–350.
16. Camenisch TD, et al. (2000) Disruption of hyaluronan synthase-2 abrogates normal cardiac morphogenesis and hyaluronan-mediated transformation of epithelium to mesenchyme. *J Clin Invest* 106:349–360.
17. Baldwin HS, Lloyd TR, Solursh M (1994) Hyaluronate degradation affects ventricular function of the early postlooped embryonic rat heart in situ. *Circ Res* 74:244–252.
18. Stennard FA, Harvey RP (2005) T-box transcription factors and their roles in regulatory hierarchies in the developing heart. *Development* 132:4897–4910.
19. Takeuchi JK, et al. (2005) Tbx20 dose-dependently regulates transcription factor networks required for mouse heart and motoneuron development. *Development* 132:2463–2474.
20. Paxton C, Zhao H, Chin Y, Langner K, Reecy J (2002) Murine Tbx2 contains domains that activate and repress gene transcription. *Gene* 283:117–124.
21. Brown CB, Boyer AS, Runyan RB, Barnett JV (1999) Requirement of type III TGF-beta receptor for endocardial cell transformation in the heart. *Science* 283:2080–2082.
22. Nakajima Y, Yamagishi T, Hokari S, Nakamura H (2000) Mechanisms involved in valvuloseptal endocardial cushion formation in early cardiogenesis: Roles of transforming growth factor (TGF)-beta and bone morphogenetic protein (BMP). *Anat Rec* 258:119–127.
23. Camenisch TD, Schroeder JA, Bradley J, Klewer SE, McDonald JA (2002) Heart-valve mesenchyme formation is dependent on hyaluronan-augmented activation of ErbB2-ErbB3 receptors. *Nat Med* 8:850–855.
24. Zoltan-Jones A, Huang L, Ghatak S, Toole BP (2003) Elevated hyaluronan production induces mesenchymal and transformed properties in epithelial cells. *J Biol Chem* 278:45801–45810.
25. Bernanke DH, Orkin RW (1984) Hyaluronidase activity in embryonic chick heart muscle and cushion tissue and cells. *Dev Biology* 106:351–359.
26. Jiao K, et al. (2003) An essential role of Bmp4 in the atrioventricular septation of the mouse heart. *Genes Dev* 17:2362–2367.
27. Bartram U, et al. (2001) Double-outlet right ventricle and overriding tricuspid valve reflect disturbances of looping, myocardialization, endocardial cushion differentiation, and apoptosis in TGF-beta (2)-knockout mice. *Circulation* 103:2745–2752.
28. Singh R, et al. (2009) Tbx20 interacts with smads to confine tbx2 expression to the atrioventricular canal. *Circ Res* 105:442–452.
29. Chi X, et al. (2005) Complex cardiac Nkx2–5 gene expression activated by noggin-sensitive enhancers followed by chamber-specific modules. *Proc Natl Acad Sci USA* 102:13490–13495.
30. Brown CO, III, et al. (2004) The cardiac determination factor, Nkx2–5, is activated by mutual cofactors GATA-4 and Smad1/4 via a novel upstream enhancer. *J Biol Chem* 279:10659–10669.

Nongenetic method for purifying stem cell–derived cardiomyocytes

Fumiyuki Hattori[1,2], Hao Chen[1,3], Hiromi Yamashita[1], Shugo Tohyama[1,3], Yu-suke Satoh[1,4], Shinsuke Yuasa[1], Weizhen Li[1], Hiroyuki Yamakawa[1,3], Tomofumi Tanaka[1,2], Takeshi Onitsuka[1,3], Kenichiro Shimoji[1,3], Yohei Ohno[1,3], Toru Egashira[1,3], Ruri Kaneda[1], Mitsushige Murata[1,3], Kyoko Hidaka[5], Takayuki Morisaki[5], Erika Sasaki[6], Takeshi Suzuki[4], Motoaki Sano[1], Shinji Makino[1], Shinzo Oikawa[2] & Keiichi Fukuda[1]

Several applications of pluripotent stem cell (PSC)-derived cardiomyocytes require elimination of undifferentiated cells. A major limitation for cardiomyocyte purification is the lack of easy and specific cell marking techniques. We found that a fluorescent dye that labels mitochondria, tetramethylrhodamine methyl ester perchlorate, could be used to selectively mark embryonic and neonatal rat cardiomyocytes, as well as mouse, marmoset and human PSC-derived cardiomyocytes, and that the cells could subsequently be enriched (>99% purity) by fluorescence-activated cell sorting. Purified cardiomyocytes transplanted into testes did not induce teratoma formation. Moreover, aggregate formation of PSC-derived cardiomyocytes through homophilic cell-cell adhesion improved their survival in the immunodeficient mouse heart. Our approaches will aid in the future success of using PSC-derived cardiomyocytes for basic and clinical applications.

Human embryonic stem cells (ESCs) and induced pluripotent stem cells (iPSCs) could prove to be an unlimited source of cardiomyocytes. Several studies have achieved directed differentiation of mouse, monkey and human ESCs into cardiomyocytes[1–3] but with variable efficiency. Some protocols describe up to 60% differentiation efficiency, but none achieve >99% of cells differentiating into cardiomyocytes without the use of genetic selection methods[4]. Transplantation of undifferentiated ESCs results in the formation of teratomas[5]. Thus, it is necessary to purify ESC-derived cardiomyocytes before transplantation.

ESC lines with various combinations of cardiomyocyte-specific reporters can be used to obtain highly pure ESC-derived cardiomyocytes[4,6–10], but this requires genetic modification of the cells. Also, discontinuous Percoll density gradient centrifugation could be used to enrich for mouse and human ESC-derived cardiomyocytes, but the purity of the cardiomyocytes in these preparations is relatively low[11,12]. Here we show that cardiomyocytes in early mouse embryos or those differentiated from pluripotent stem cells (PSCs) have high mitochondrial content and can be purified without the need for genetic modification, using fluorescent dyes that label mitochondria.

RESULTS

Characterization of mitochondrial dyes

In primary cultures of neonatal rat heart cells stained with MitoTracker Red (Invitrogen) the fluorescence intensity of cardiomyocytes was much higher compared to that of non-myocytes (**Fig. 1a**). MitoTracker Red and tetramethylrhodamine methyl ester perchlorate (TMRM) specifically accumulated in both the subsarcomeric mitochondria, located around the nucleus and in the intermyofibrillar mitochondria (**Fig. 1a** and **Supplementary Fig. 1**). To confirm specific mitochondrial staining of MitoTracker dyes, we stained neonatal rat cardiomyocytes with MitoTracker Red and JC-1 (a mitochondrial voltage-sensitive dye; **Supplementary Fig. 2**).

Fluorescence-activated cell sorter (FACS) analysis of cells dissociated from neonatal heart revealed three main populations (**Fig. 1b**). We sorted the populations with the highest (designated as fraction 1), the middle (fraction 2) and the lowest (fraction 3) fluorescence intensity and cultured them separately. All the cells in fraction 1 showed rhythmic beating and were immunostained with an antibody to α-actinin (**Fig. 1c**), indicating they were cardiomyocytes. We identified very few cardiomyocytes in fraction 2 (**Fig. 1c**). Fraction 3 consisted of red blood cells and dead cells. We confirmed the neonatal rat cardiomyocyte content in fraction 1 by immunofluorescence staining for α-actinin to be 99.4 ± 0.6% (**Fig. 1d**), and the yield was approximately 5×10^5 cells from a single heart.

Next, we compared the efficacy of various mitochondrial dyes for separating the neonatal rat cardiomyocyte population from the nonmyocytes and found that TMRM was the most effective (**Fig. 1e,f**). We then evaluated the washout efficiencies of the dyes and found that TMRM disappeared completely within 24 h, whereas

[1]Department of Regenerative Medicine and Advanced Cardiac Therapeutics, Keio University School of Medicine, Tokyo, Japan. [2]Asubio Pharma Co., Ltd., Osaka, Japan. [3]Division of Cardiology, Department of Medicine, Keio University School of Medicine, Tokyo, Japan. [4]Division of Basic Biological Sciences, Faculty of Pharmacy, Keio University, Tokyo, Japan. [5]Department of Bioscience, National Cardiovascular Center Research Institute, Osaka, Japan. [6]Laboratory of Applied Developmental Biology, Marmoset Research Department, Central Institute for Experimental Animals, Kanagawa, Japan. Correspondence should be addressed to K.F. (kfukuda@sc.itc.keio.ac.jp).

RECEIVED 10 AUGUST; ACCEPTED 15 OCTOBER; PUBLISHED ONLINE 29 NOVEMBER 2009; DOI:10.1038/NMETH.1403

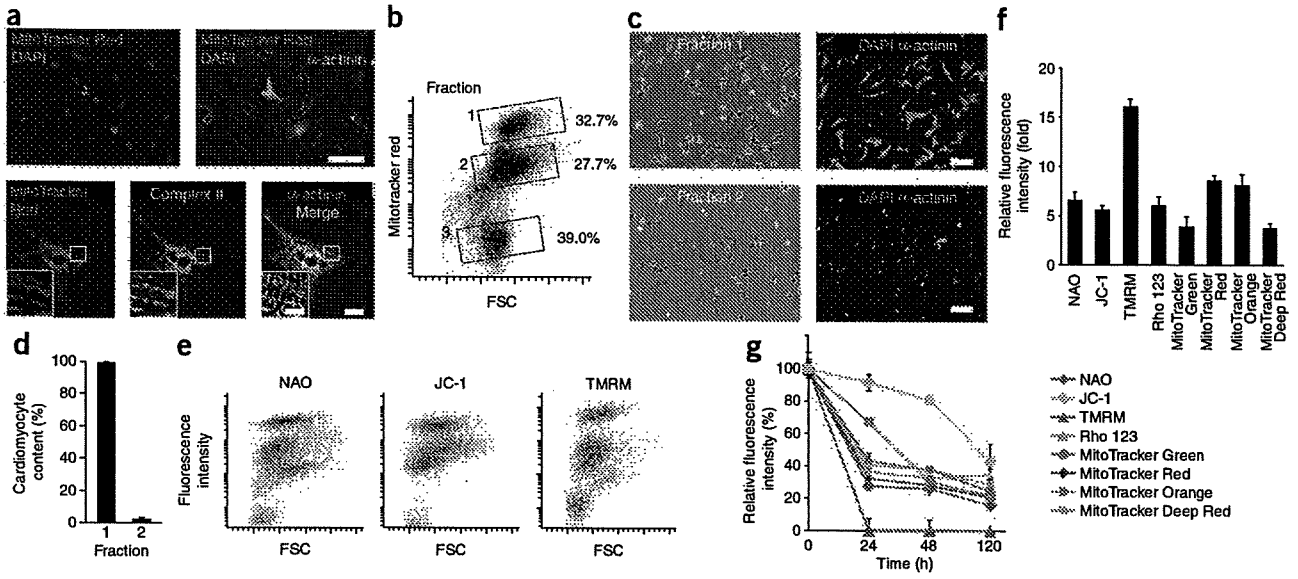

Figure 1 | Mitochondrial dyes for cardiomyocyte purification. (**a**) Fluorescence images of neonatal rat cardiomyocytes prestained with MitoTracker Red and immunostained for α-actinin (top) or prestained with MitoTracker Red and immunostained for mitochondrial electron transfer chain complex II (complex II) and α-actinin (bottom). DAPI, nuclear stain. Scale bars, 100 μm (top); 20 μm (bottom); and 10 μm (bottom inset). (**b**) FACS analysis of neonatal rat heart–derived cells stained with MitoTracker Red. The sorted cells were divided into fractions 1–3 (boxed). FSC, forward scatter. (**c**) Immunofluorescence staining for α-actinin of cells from fractions 1 and 2. Blue, DAPI staining. Scale bars, 100 μm. (**d**) Cardiomyocyte content in fractions 1 and 2. Data are shown as mean ± s.d. (n = 3). (**e**) Representative FACS plots of dissociated cells from neonatal rat heart stained with mitochondrial dyes. (**f**) Relative fluorescence intensity of the indicated mitochondrial dyes in fractions 1 versus 2. Data are shown as mean ± s.d. (n = 3). (**g**) Washout of the indicated mitochondrial dyes from neonatal rat cardiomyocytes. Data are shown as mean ± s.d. (n = 3).

other dyes remained for at least 5 d (**Fig. 1g** and **Supplementary Fig. 3a**). TMRM and JC-1 at 100 nM did not affect cell viability using 3-(4,5-dimethyl-thiazol-2-yl)-2,5-diphenyltetrazolium bromide (MTT) assay, whereas other dyes affected viability differently (**Supplementary Fig. 3b**). Based on these results, we selected TMRM for subsequent experiments.

Purification of cardiomyocytes from heart and whole embryos

To investigate the mitochondrial content of cardiomyocytes at different developmental stages, we performed FACS analysis of rat hearts at embryonic day 11.5 (E11.5) to postnatal day 8 (P8); the hearts had been dissociated and labeled with TMRM (**Fig. 2a**). The mean ratio of TMRM fluorescence in fraction 1 to fraction 2 gradually increased with increasing embryonic stage and rapidly after birth (**Fig. 2b**). FACS analysis followed by immunofluorescence staining confirmed over 99% cardiomyocyte purity at all stages (**Fig. 2c,d**).

We then stained live embryos (E11.5 and E12.5) with TMRM. The heart showed markedly stronger fluorescence compared with other tissues (**Fig. 2e** and **Supplementary Video 1**). Intraplacental injection of MitoTracker Red also resulted in the strongest accumulation of fluorescence in the heart via embryonic circulation. However, other tissues had much weaker fluorescence (**Supplementary Fig. 4**).

To assess why there was strong TMRM fluorescence in the embryonic heart, we compared expression levels of complex I–V of the 36 kDa mitochondrial outer membrane protein porin (also known as the voltage-dependent anion channel) and of heat shock protein 70 between cardiac and various noncardiac tissues in rat E12.5 embryos; we detected markedly stronger expression in the myocardium (**Supplementary Fig. 5**). Furthermore, immunostaining of the fetal heart area for α-actinin, manganese superoxide dismutase (MnSOD) and platelet endothelial cell adhesion molecule (PECAM) (markers of cardiomyocytes, mitochondria and the endothelium, respectively), revealed that MnSOD immunostaining overlapped that for α-actinin but not for PECAM (**Fig. 2f**). Taken together, the accumulation of fluorescent dyes that label mitochondria may reflect high mitochondria abundance in the heart.

Next, we treated dissociated cells obtained from E11.5 to E13.5 whole rat embryos with TMRM and analyzed them on a FACS (**Fig. 2g**). Some cells in this preparation were autofluorescent, which was due to the presence of lipopigments and flavins[13]. To obtain only TMRM-fluorescent cells and eliminate contamination by autofluorescent cells, we adopted pseudo-two-dimensional separation (**Fig. 2g** and Online Methods). We isolated populations with the highest TMRM-fluorescence from dispersed cells of E11.5, E12.5 and E13.5 whole rat embryos. The sorted cells from E11.5 embryos were immunostained for α-actinin (purity 99%, n = 3 embryos; yield, ~5 × 10^3 cells per embryo). We obtained similar results with E12.5 and E13.5 embryos. At these embryonic stages (E11.5–E13.5), the embryos contain skeletal myoblasts only and not mature myotubes. We found that mature skeletal myotubes, which could not pass through the FACS, could be marked with TMRM, whereas skeletal myoblasts, which do pass through the FACS, were not marked by TMRM (**Supplementary Fig. 6**).

Purification of PSC-derived cardiomyocytes

We first observed cardiomyocytes differentiated from mouse ESCs on day 7 of differentiation; the cells had marked TMRM accumulation. After TMRM staining, we fixed the cells and immunostained them for Nkx2.5 and α-actinin (**Fig. 3a**). The Nkx2.5– and α-actinin–positive areas and TMRM-positive area in the mouse

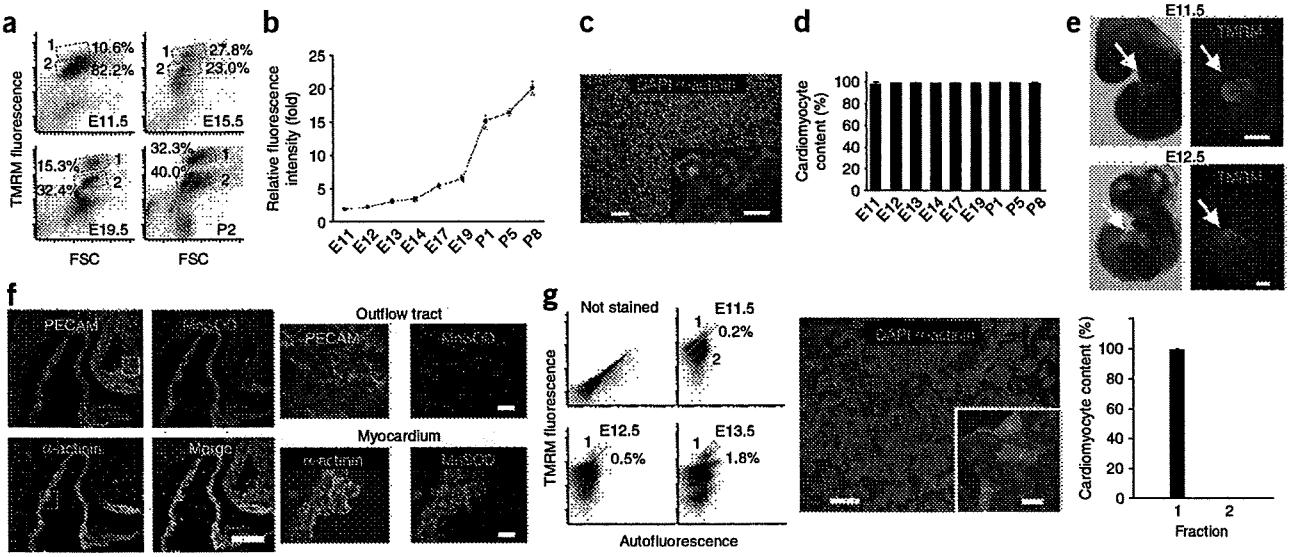

Figure 2 | Purification of cardiomyocytes from embryonic heart and whole embryo. (**a**) Representative FACS analysis of TMRM-stained rat embryonic heart cells at the indicated ages. Fractions 1 and 2 were typical gates for cardiomyocytes and noncardiomyocytes, respectively. (**b**) Relative fluorescence intensity of fraction 1 versus fraction 2 in the developing rat heart. Data are shown as mean ± s.d. (n = 3). (**c**) Immunofluorescence staining for α-actinin in the fraction 1 gated cells from E11.5 rat heart. (**d**) Cardiomyocyte content of the fraction 1-gated cells obtained from E11.5–P8 rat hearts. Data are shown as mean ± s.d. (n = 3). (**e**) Bright field (left) and fluorescence (right) images of whole rat embryos of indicated ages. (**f**) Immunofluorescence staining of rat E11.5 embryo for the indicated markers, PECAM, α-actinin and MnSOD. Images show pericardiac area (left four) and magnification of the boxed areas is shown on the right. (**g**) FACS analysis (left) of dissociated cells from whole embryos in the absence (not stained) or presence of TMRM at the indicated stages. Boxes indicate fractions 1 and 2; percentages of fraction 1 cells are shown. Immunofluorescence staining (middle) for α-actinin in the cells obtained from fraction 1 of E11.5 embryos. Cardiomyocyte content of fractions 1 and 2 at E11.5 is shown (right). Data are shown as mean ± s.d. (n = 3). Scale bars, 100 μm (**c**,**g**,**e**); 200 μm (**f** left); and 20 μm (**c** inset, **f** right, **g** inset).

ESC–derived cardiomyocytes were colocalized completely, although the intracellular localization of TMRM, Nkx2.5 and α-actinin was clearly different. Notably, TMRM dissociated rapidly into the bulk solution compared with other dyes upon fixation (**Supplementary Fig. 7**), indicating that there is likely to be no effect of TMRM on subsequent immunohistochemical analysis.

We applied pseudo–two-dimensional FACS analysis to the embryoid body–derived cells (**Fig. 3b**). We first observed fraction 1 cells 7 d after embryoid body formation. Both the ratio of the mean TMRM fluorescence in fraction 1 (cardiomyocytes) to fraction 2 (noncardiomyocytes) and the percentage of cells in fraction 1 increased gradually until day 15 (**Fig. 3c,d**), suggesting that the best time for obtaining mouse ESC–derived cardiomyocytes was at day 15.

We sorted approximately 5×10^5 to 9×10^5 cells from day 15 embryoid bodies. The viability of the sorted cells was 99.1 ± 1.5%, as confirmed by trypan blue staining (**Supplementary Fig. 8**). This high viability may be due to the fact that the cells were sorted based on TMRM accumulation (and thus contained active mitochondria). We cultured the sorted cells for 7 d to allow the cells to attach to the substrate and to elongate (Online Methods). Immunofluorescence staining for α-actinin and Nkx2.5 in three independent experiments confirmed that these cells were high-purity cardiomyocytes (99.5 ± 0.3%; **Fig. 3e**). We obtained >99% pure ESC-derived cardiomyocytes from day 12–25 embryoid bodies (**Fig. 3f**). We also obtained highly pure cardiomyocytes from mouse iPSCs (**Fig. 3g,h**).

To investigate the possibility of isolating cardiac progenitor cells, we stained whole E7.5 and E7.75 embryos. We found that TMRM faintly, but distinctly, marked the cardiac crescent, which contains cardiomyogenic precursor cells, indicating a possible applicability of our method to obtaining progenitor cells. Next, we carried out time-lapse fluorescence microscopy on attached mouse embryoid bodies stained with TMRM (**Supplementary Fig. 9**). We first observed TMRM-positive cells on day 6.5. Fluorescence in these cells increased gradually between days 6.5 and 7 and they started beating on day 7.0. In contrast, TMRM-negative cells did not beat during the experiments. We then performed FACS analysis on dissociated cells obtained from day 3–6.5 embryoid bodies and stained with TMRM. There were no cells in fraction 1. The higher TMRM-fluorescence cells in fraction 2 from day 3 and 4 embryoid bodies did not differentiate into cardiomyocytes, even after subsequent culture of attached cells for up to 8 d. In the case of day 6.5 embryoid bodies, some of the isolated cells differentiated into cardiomyocytes upon subsequent culture for 3 d. We also stained *Nkx2.5-GFP* knock-in mouse ESCs[6], which we and others have used frequently to isolate cardiomyocytes. After embryoid body formation, we first observed GFP fluorescence on day 7, whereas we observed TMRM staining on day 6.5 (**Supplementary Fig. 10**). Our observations indicate that our method can be used to purify differentiated cardiomyocytes but not cardiac progenitor cells.

We differentiated common marmoset ESCs, human ESCs and human iPSCs into cardiomyocyte-containing embryoid bodies by conventional floating cell culture. We transferred the embryoid bodies into the cell-attachment dishes with 10 nM TMRM. Beating embryoid bodies had extremely high TMRM fluorescence compared with that of nonbeating embryoid bodies derived from marmoset and human ESCs (**Fig. 4a**). Then we dispersed embryoid body–derived cells, stained them with TMRM and analyzed them on a FACS (**Fig. 4b**). We fixed sorted human

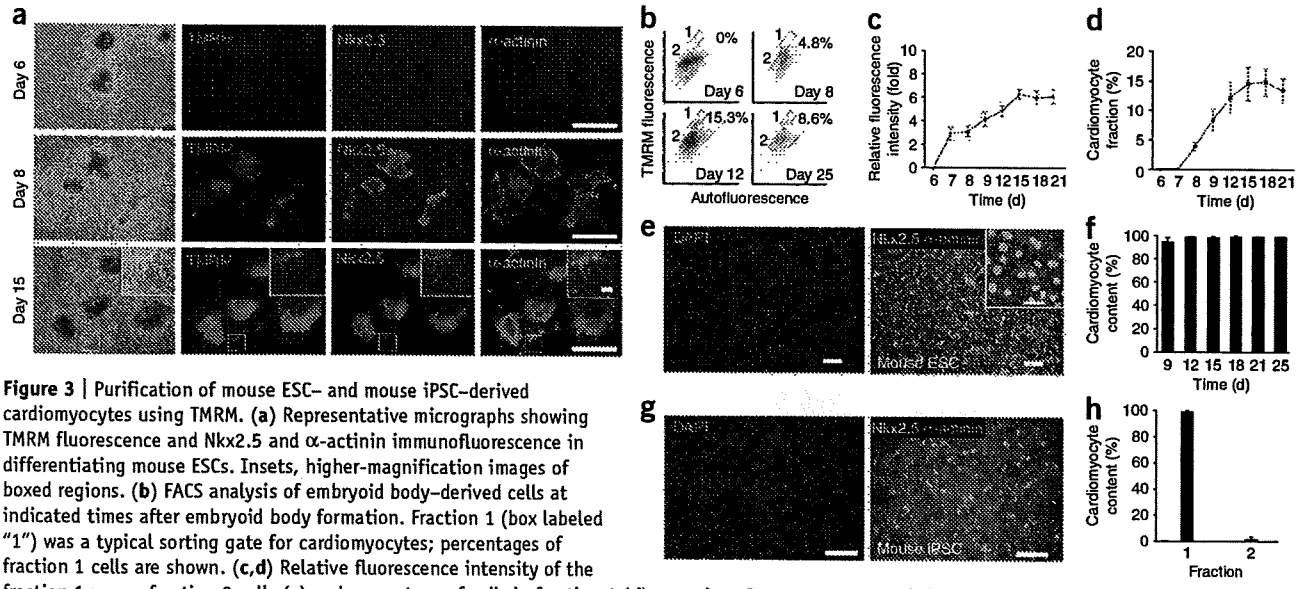

Figure 3 | Purification of mouse ESC- and mouse iPSC-derived cardiomyocytes using TMRM. (**a**) Representative micrographs showing TMRM fluorescence and Nkx2.5 and α-actinin immunofluorescence in differentiating mouse ESCs. Insets, higher-magnification images of boxed regions. (**b**) FACS analysis of embryoid body–derived cells at indicated times after embryoid body formation. Fraction 1 (box labeled "1") was a typical sorting gate for cardiomyocytes; percentages of fraction 1 cells are shown. (**c**,**d**) Relative fluorescence intensity of the fraction 1 versus fraction 2 cells (**c**) and percentage of cells in fraction 1 (**d**) over time. Data are mean ± s.d. ($n = 3$). (**e**–**h**) Immunofluorescence staining for Nkx2.5 and α-actinin in cultured fraction 1 cells sorted from day 15 embryoid bodies differentiated from mouse ESCs (**e**) and from mouse iPSCs (**g**); and cardiomyocyte content in cultured cells sorted from day 9–25 embryoid bodies differentiated from mouse ESCs (**f**) and in cultured cells sorted from day 15 embryoid bodies differentiated from mouse iPSCs (**h**). Data are mean ± s.d. ($n = 3$). Scale bars, 1 mm (**a**); and 100 μm (**a** inset, **e**,**g**).

cells in fraction 1, immunostained them for Nkx2.5 and subjected them to a second FACS analysis. The results showed that over 99.9% of cells in fraction 1 were cardiomyocytes (**Fig. 4c**). Furthermore, we compared expression of cardiac and noncardiac genes in human ESC–derived cardiomyocytes isolated by our method and in unpurified cells from embryoid bodies using real-time PCR. We observed a marked increase in the expression of myocardial genes and a decrease in the expression of nonmyocardial genes in purified human ESC–derived cardiomyocytes (**Supplementary Fig. 11**).

We also cultured the sorted cells for 5 d and immunostained them for Nkx2.5 and α-actinin (**Fig. 4d**). Common marmoset ESC, human ESC and human iPSC fraction 1 comprised 99.0 ± 1.0%, 99.0 ± 0.9% and 99.3 ± 0.2% cardiomyocytes, respectively; in contrast, fraction 2 had 2.3 ± 0.6%, 2.5 ± 0.2% and 1.7 ± 1.6% cardiomyocytes, respectively (**Fig. 4e**). To estimate the acquisition efficiency in the sorting experiments, we compared by FACS analysis the cardiomyocyte fraction obtained by TMRM with that obtained by immunofluorescence staining for α-actinin. The number of cardiomyocytes isolated by TMRM staining was 60–90% of the number defined by α-actinin staining (**Supplementary Fig. 12**). To rule out the possibility of skeletal muscle contamination in the sorted cardiomyocyte population, we extracted total mRNA from sorted cardiomyocytes and evaluated it for *myoD* expression using real-time PCR. We confirmed that there was no amplification of *myoD* (**Supplementary Fig. 13**).

No teratoma formation

We cultured the purified mouse ESC-derived cardiomyocytes and noncardiomyocytes for 7 d and found that although noncardiomyocytes formed piled-up colonies, in which some cells

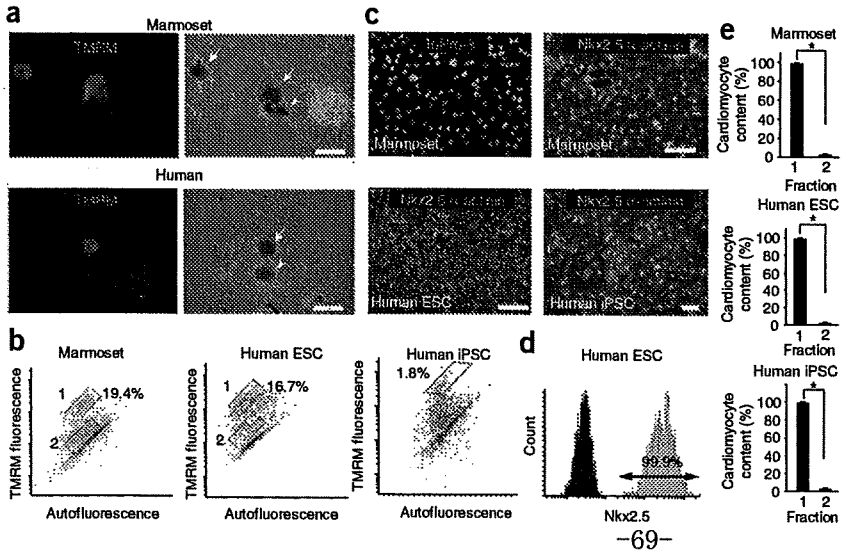

Figure 4 | Purification of PSC-derived cardiomyocytes in human and marmoset. (**a**) TMRM fluorescence (left) and phase contrast (right) images of marmoset and human embryoid bodies containing beating cardiomyocytes. Arrows, beating areas; arrowheads, nonbeating areas. (**b**) FACS separation of TMRM-stained cardiomyocytes derived from common marmoset ESCs, human ESCs and human iPSCs. Fractions 1 and 2 are boxed; percentages of fraction 1 cells are shown. (**c**) Immunofluorescence staining of fraction 1 cells for α-actinin and Nkx2.5. ToPro-3 represents nuclear staining. (**d**) Histogram showing immunodetection of Nkx2.5 (gray) and negative control (without first antibody; black) in sorted human ESC–derived fraction 1 cells. (**e**) The cardiomyocyte content of fractions 1 and 2 in common marmoset ESCs, human ESCs and human iPSCs. Data are mean ± s.d. ($n = 3$). *$P < 0.01$ (Student t-test). Scale bars, 500 μm (**a**); and 100 μm (**c**).

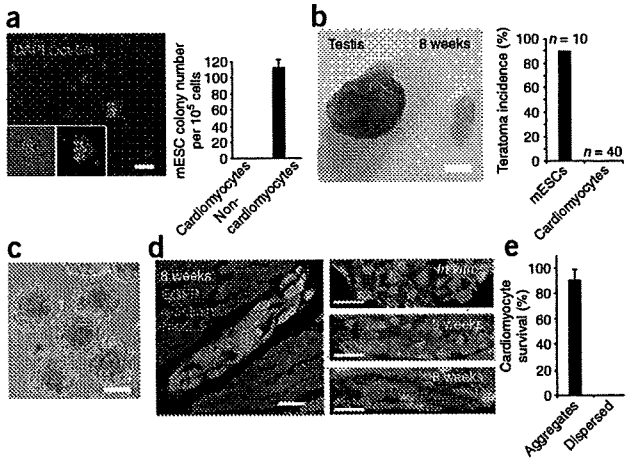

Figure 5 | Transplantation of purified mouse ESC-derived cardiomyocytes. (**a**) Immunofluorescence staining for Oct3/4 (red) in the sorted cells from the noncardiac fraction (left), and numbers of mouse ESC-like colonies obtained from 10^5 sorted cells (right). Data are mean ± s.d. ($n = 3$). (**b**) Transplantation of 250 undifferentiated mouse ESCs into testes resulted in teratoma formation (testis), whereas transplantation of 1.9×10^5 purified mouse ESC-derived cardiomyocytes did not (8 weeks). Incidence of teratoma formation was quantified (right). (**c**) Phase contrast image of mouse cardiomyocyte aggregates. (**d**) Immunofluorescence staining of engrafted mouse cardiomyocyte aggregates for α-actinin and Nkx2.5 8 weeks after transplantation (left); transplanted cells expressed EGFP. Mouse ESC-derived cardiomyocytes *in vitro* and 3 and 8 weeks after transplantation immunostained for Nkx2.5 and α-actinin (right). (**e**) Transplanted mouse ESC-derived cardiomyocyte survival. Data are shown as mean ± s.d. ($n = 5$). Scale bars, 100 μm (**a**,**c**); 5 mm (**b**); and 20 μm (**d**).

were positive for Oct3/4, the cardiomyocytes did not (**Fig. 5a**). Further, we transplanted 1.9×10^5 aggregated mouse ESC-derived cardiomyocytes and 250 undifferentiated mouse ESCs as a control into the testes of immunocompromised nonobese diabetic–severe combined immunodeficient (NOD-SCID) mice. Two months later, 90% of the control mice developed teratomas (9 of 10 mice), but we did not detect teratomas in any of the mice transplanted with purified mouse ESC-derived cardiomyocytes (0 of 40 mice) (**Fig. 5b**). We tried to verify that there was no teratoma formation in the heart by directly injecting mouse ESC-derived cardiomyocytes (1×10^5) into the myocardium of five NOD-SCID mice immediately after sorting. Two months later, we found few (<1%) of the transplanted cardiomyocytes in the heart (data not shown).

To understand the mechanism underlying this cell loss, we injected purified and MitoTracker Red–labeled neonatal rat cardiomyocytes into the left ventricular free wall of *ex vivo*–perfused hearts. We found one-third to one-half of injected cells in the postperfusion solution, indicating that the neonatal rat cardiomyocytes were washed out within the first 10 min (**Supplementary Fig. 14**). Next, we compared the tissue adhesiveness of purified mouse ESC-derived cardiomyocytes and mouse embryonic fibroblasts (MEFs) by counting cells in continuous sections of whole ventricles 24 h after injection into the left ventricular free walls. We found that less than 1% of the grafted ESC-derived cardiomyocytes had adhered to the host myocardium, compared with 50% of MEFs.

Transplantation of PSC-derived cardiomyocytes

From the above observations, we reasoned that loss of transplanted ESC-derived cardiomyocytes may be due to rapid washout and low adhesiveness of the cells. Because ESC-derived cardiomyocytes existed as homophilic cell aggregates (diameter, 100–500 μm) in mouse, marmoset and human embryoid bodies (**Supplementary Fig. 15**), we suspected that re-aggregated purified ESC-derived cardiomyocytes may be more resistant to rapid washout. We generated cardiomyocyte aggregates by seeding 313–10,000 purified mouse ESC-derived cardiomyocytes onto nonadhesive 96-well plates. One day after seeding, the cells adhered to each other, aggregated and started synchronized beating; 5 d later, cardiomyocyte aggregates formed with diameters of 100–450 μm (**Fig. 5c**, **Supplementary Fig. 16** and **Supplementary Video 2**). Propidium iodide staining revealed that a high proportion of re-aggregated mouse ESC-derived cardiomyocytes were viable (98.8 ± 0.2% of seeded cells; **Supplementary Fig. 16**).

We transplanted mouse cardiomyocyte aggregates into the ventricular free walls of NOD-SCID mice and killed the mice at 3 and 8 weeks ($n = 5$ for both groups). We observed no teratoma formation in either group. Immunofluorescence staining revealed that cell aggregates positive for the tracers Nkx2.5 and α-actinin were located in the left ventricle (**Fig. 5d**). The number of cells that survived in the heart was greater than 90% (**Fig. 5e**). Furthermore, we repeated these experimental procedures using purified human ESC-derived cardiomyocytes (**Supplementary Video 3**). Two months after transplantation, we detected a large amount of human myocardial tissue in NOD-SCID mouse heart (**Supplementary Fig. 17**).

Finally, we investigated which autoparacrine factors are important for the survival of ESC-derived cardiomyocytes. Human cardiomyocyte aggregates remained viable under serum-free culture conditions; moreover, their diameters increased by approximately twofold by day 25. Supplementation of the cultures with physiological concentrations of basic fibroblast growth factor (bFGF), epidermal growth factor (EGF), platelet-derived growth factor beta dimer (PDGF-BB) and endothelin-1 (ET-1) strongly enhanced the growth of the cardiomyocyte aggregates (**Supplementary Fig. 18a** and **Supplementary Video 4**). We confirmed expression of these growth factors and their receptors by real-time PCR (probe and primer sets are listed in **Supplementary Table 1**). We also confirmed that these growth factors were expressed in adult human and mouse hearts (**Supplementary Fig. 18b**). Autoparacrine stimulation with these growth factors may be one reason why grafted cardiomyocyte aggregates survived and grew in the host myocardium.

DISCUSSION

Our method for cardiomyocyte isolation has two advantages. First, it does not require genetic modification of the cells. Genetic modifications using nonviral or viral systems have several disadvantages: extrinsic genes may be silenced, the number of integration events in one cell is difficult to control, targeted integration is not straightforward, and line selection as well as verification of proper expression of extrinsic genes[14] is time-consuming. Furthermore, genetic modification carries risks such as possible tumor formation[15–17]. Second, our method is likely to be widely applicable. We demonstrated that it may be used to purify ESC-derived cardiomyocytes in four species, including human,

and that it is also applicable to mouse and human iPSCs. High abundance of cellular mitochondria is likely to be a common characteristic of cardiomyocytes irrespective of species. In contrast, most genetic modifications require species-specific constructs. Our simple purification strategy should facilitate basic studies using embryonic heart and stem cell–derived cardiomyocytes; furthermore, this strategy can also allow isolation of noncardiomyocytes, which may open up new approaches to studying developmental interactions.

The ESC-derived cardiomyocytes purified using our method did not induce teratoma formation in either the heart or testes. Although from the viewpoint of clinical safety, further studies using large animal models with a much larger number of ESC-derived cardiomyocytes will be required, we believe that our purification method may have considerable advantages over existing methods for eventual clinical translation as well.

Our results suggest that induction of mitochondrial biogenesis begins shortly before beating of cardiomyocytes. This indicates the tight relationship between cardiomyogenesis and mitochondrial biogenesis. A combination of our strategy and other marking techniques for cardiac progenitor cells may facilitate study in this field.

Unpurified fetal and neonatal rat cardiomyocytes and bone marrow mesenchymal and ESC-derived cardiomyocytes have been shown to survive in the recipient heart[18–20]. In contrast, purified and dispersed cardiomyocytes differentiated from ESCs did not achieve a high survival rate[5]. Re-aggregation augmented the long-term survival of purified mouse and human ESC–derived cardiomyocytes. Our results indicate that ESC-derived cardiomyocytes might be highly anchorage-dependent, and that homophilic cell-to-cell adhesion and autoparacrine signaling may be important factors contributing to their survival.

METHODS

Methods and any associated references are available in the online version of the paper at http://www.nature.com/naturemethods/.

Note: Supplementary information is available on the Nature Methods website.

ACKNOWLEDGMENTS

Human ESCs were a gift of N. Nakatsuji at the Department of Development and Differentiation, Institute for Frontier Medical Sciences, Kyoto University. Human and mouse iPSCs were a gift of S. Yamanaka at the Center for iPS Cell Research and Application, Institute for Integrated Cell-Material Sciences, Kyoto University. Mouse ESCs were a gift of H. Niwa at the Laboratory of Pluripotent Cell Studies, RIKEN Center for Developmental Biology. This study was supported in part by research grants from the Ministry of Education, Science and Culture, Japan, and by the Program for Promotion of Fundamental Studies in Health Science of the National Institute of Biomedical Innovation.

AUTHOR CONTRIBUTIONS

F.H. designed the whole study. F.H. performed most experiments and wrote the manuscript. H.C. participated in cell-sorting experiments and prepared cells. H.Yamashita participated in cell-sorting experiments, PCR experiments, immunofluorescent staining, animal experiments and preparing cells. S.T., Y.S., W.L., T.T., T.O., K.S., Y.O. and T.E. participated in cell preparations. H.Yamakawa and M.M. participated in heart perfusion experiments. K.H. and T.M. provided the *Nkx2.5 knock-in* ESCs. S.Y., M.M., R.K., M.S., S.M. and S.O. provided advice. E.S. provided cmESCs. T.S. supervised Y.S. K.F. provided advice, obtained the budget and supervised the project.

COMPETING INTERESTS STATEMENT

The authors declare competing financial interests: details accompany the full-text HTML version of the paper at http://www.nature.com/naturemethods/.

Published online at http://www.nature.com/naturemethods/.
Reprints and permissions information is available online at http://npg.nature.com/reprintsandpermissions/.

1. Yuasa, S. *et al.* Transient inhibition of BMP signaling by Noggin induces cardiomyocyte differentiation of mouse embryonic stem cells. *Nat. Biotechnol.* **23**, 607–611 (2005).
2. Nemir, M., Croquelois, A., Pedrazzini, T. & Radtke, F. Induction of cardiogenesis in embryonic stem cells via downregulation of Notch1 signaling. *Circ. Res.* **98**, 1471–1478 (2006).
3. Mummery, C. *et al.* Differentiation of human embryonic stem cells to cardiomyocytes: role of coculture with visceral endoderm-like cells. *Circulation* **107**, 2733–2740 (2003).
4. Anderson, D. *et al.* Transgenic enrichment of cardiomyocytes from human embryonic stem cells. *Mol. Ther.* **15**, 2027–2036 (2007).
5. Kolossov, E. *et al.* Engraftment of engineered ES cell-derived cardiomyocytes but not BM cells restores contractile function to the infarcted myocardium. *J. Exp. Med.* **203**, 2315–2327 (2006).
6. Hidaka, K. *et al.* Chamber-specific differentiation of Nkx2.5-positive cardiac precursor cells from murine embryonic stem cells. *FASEB J.* **17**, 740–742 (2003).
7. Fijnvandraat, A.C. *et al.* Cardiomyocytes purified from differentiated embryonic stem cells exhibit characteristics of early chamber myocardium. *J. Mol. Cell. Cardiol.* **35**, 1461–1472 (2003).
8. Gassanov, N., Er, F., Zagidullin, N. & Hoppe, U.C. Endothelin induces differentiation of ANP-EGFP expressing embryonic stem cells towards a pacemaker phenotype. *FASEB J.* **18**, 1710–1712 (2004).
9. Huber, I. *et al.* Identification and selection of cardiomyocytes during human embryonic stem cell differentiation. *FASEB J.* **21**, 2551–2563 (2007).
10. Klug, M.G., Soonpaa, M.H., Koh, G.Y. & Field, L.J. Genetically selected cardiomyocytes from differentiating embronic stem cells form stable intracardiac grafts. *J. Clin. Invest.* **98**, 216–224 (1996).
11. Laflamme, M.A. *et al.* Cardiomyocytes derived from human embryonic stem cells in pro-survival factors enhance function of infarcted rat hearts. *Nat. Biotechnol.* **25**, 1015–1024 (2007).
12. Xu, C., Police, S., Hassanipour, M. & Gold, J.D. Cardiac bodies: a novel culture method for enrichment of cardiomyocytes derived from human embryonic stem cells. *Stem Cells Dev.* **15**, 631–639 (2006).
13. Monici, M. Cell and tissue autofluorescence research and diagnostic applications. *Biotechnol. Annu. Rev.* **11**, 227–256 (2005).
14. Gropp, M. & Reubinoff, B. Lentiviral vector-mediated gene delivery into human embryonic stem cells. *Methods Enzymol.* **420**, 64–81 (2006).
15. Tsukahara, T. *et al.* Murine leukemia virus vector integration favors promoter regions and regional hot spots in a human T-cell line. *Biochem. Biophys. Res. Commun.* **345**, 1099–1107 (2006).
16. Recchia, A. *et al.* Retroviral vector integration deregulates gene expression but has no consequence on the biology and function of transplanted T cells. *Proc. Natl. Acad. Sci. USA* **103**, 1457–1462 (2006).
17. Woods, N.B. *et al.* Lentiviral vector transduction of NOD/SCID repopulating cells results in multiple vector integrations per transduced cell: risk of insertional mutagenesis. *Blood* **101**, 1284–1289 (2003).
18. van Laake, L.W. *et al.* Human embryonic stem cell-derived cardiomyocytes survive and mature in the mouse heart and transiently improve function after myocardial infarction. *Stem Cell Rev.* **1**, 9–24 (2007).
19. Reinecke, H., Zhang, M., Bartosek, T. & Murry, C.E. Survival, integration, and differentiation of cardiomyocyte grafts: a study in normal and injured rat hearts. *Circulation* **100**, 193–202 (1999).
20. Hattan, N. *et al.* Purified cardiomyocytes from bone marrow mesenchymal stem cells produce stable intracardiac grafts in mice. *Cardiovasc. Res.* **65**, 334–344 (2005).

ONLINE METHODS

Mouse, common marmoset and human PSCs. Mouse ESCs were obtained from Laboratory of Pluripotent Cell Studies, RIKEN Center for Developmental Biology. Common marmoset ESCs (cmESCs) were obtained from Central Institute for Experimental Animals. The human ESC lines (khESC-1, 2 and 3) were obtained from Department of Development and Differentiation, Institute for Frontier Medical Sciences, Kyoto University and were used in conformity with The Guidelines for Derivation and Utilization of Human Embryonic Stem Cells of the Ministry of Education, Culture, Sports, Science and Technology, Japan. Mouse (iPS-MEF-Ng-20D-17) and human (253G4) iPSCs were obtained from Center for iPSC Research and Application, Kyoto University.

Animals. All animals including pregnant and neonatal Wistar rats, and NOD-SCID mice (10 weeks old, male), were purchased from Japan CLEA.

All experimental procedures and protocols were approved by the Animal Care and Use Committees of the Keio University and conformed to the US National Institutes of Health Guide for the Care and Use of Laboratory Animals.

Reagents. MitoTracker dyes (Deep Red, Red, Orange and Green), TMRM, 5,5′,6,6′-tetrachloro-1,1′,3,3′-tetraethylbenzimidazolylcarbocyanine iodide (JC-1), nonyl acridine orange (NAO) and Rhodamine 123 were purchased from Invitrogen. These mitochondria-selective fluorescent dyes can be divided into the Nernstian or non-Nernstian dye groups. The former, including TMRM, can enter into and exit from the mitochondrial matrix freely depending on the mitochondrial membrane potential. In contrast, non-Nernstian dyes such as the MitoTracker dyes cannot exit freely[21]. This characteristic difference may reflect their toxicities and can be used case by case for research, for example, non-Nernstian dyes are used for long-term staining.

The mouse monoclonal antibody to α-actinin (used at 1:400 dilution) was purchased from Sigma-Aldrich. The goat polyclonal antibody to GATA-4 (C-20) and the goat polyclonal antibody for Nkx2.5 (N-19) were purchased from Santa Cruz biotechnology. The mouse monoclonal antibody for SdhB (1:100), Alexa Fluor 488 donkey anti-mouse IgG antibody and Alexa Fluor 546 donkey anti-goat immunoglobulin gamma (IgG) were purchased from Invitrogen.

Maintenance of mouse, marmoset and human PSCs. We maintained mouse ESCs and iPSCs on gelatin-coated dishes in Glasgow Minimum Essential Medium (Sigma) supplemented with 10% FBS (FBS; Equitechbio), 0.1 mM MEM Non-Essential Amino Acids solution (Sigma), 2 mM L-glutamine (Sigma), 0.1 mM β-mercaptoethanol (Sigma) and 2,000 U ml^{-1} mouse LIF (Chemicon). We maintained cmESCs on mouse embryonic fibroblasts in Knockout Dulbecco's Modified Eagle's Medium (KO-DMEM; Invitrogen) supplemented with 20% Knockout Serum Replacement (KSR; Invitrogen), 0.1 mM MEM Non-Essential Amino Acids solution, 2 mM L-glutamine, 0.1 mM β-mercaptoethanol and 4 ng ml^{-1} basic fibroblast growth factor (bFGF; Wako Pure Chemical). We maintained human ESCs and iPSCs similarly to cmESCs, except that Dulbecco's Modified Eagle's Medium/Nutrient Mixture F-12 Ham 1:1 (DMEM-F12; Sigma) was used instead of KO-DMEM.

Differentiation of mouse PSC–derived cardiomyocytes. We performed *in vitro* differentiation of mouse ESCs and iPSCs as described below. We collected mouse PSCs with 0.25% trypsin-EDTA and dissociated them. Seventy-five cells were formed to one embryoid body in one hanging drop with alpha-modified Eagle medium (αMEM; Sigma) supplemented with 10% FBS (Equitechbio). On day 2, we transferred embryoid bodies into floating culture plate with new medium. Four to five days after differentiation, floating embryoid bodies were transferred into attachment culture with nonserum culture medium: αMEM supplemented with insulin-transferrin-selenium (ITS; Sigma). Typically, beating cells appeared on day 7. Embryoid bodies were used for purification experiments between days 12 and 25.

Differentiation of cmESC–derived cardiomyocytes. We performed differentiation of cmESCs as follows. The colonies were detached with 0.1% type three collagenase (Worthington Biochemical) and cultured in cmESC medium lacking bFGF or αMEM and supplemented with 10% FBS (SAFC Biosciences) and 0.1 mM β-mercaptoethanol in bacterial Petri dishes to form embryoid bodies. Typically, 5–20% of embryoid bodies contained beating cells. Embryoid bodies were washed three times with αMEM between days 18 and 25, and cultured with αMEM supplemented with ITS. Embryoid bodies were used for purification experiments between days 30 and 50.

Differentiation of human PSC–derived cardiomyocytes. We grew the detached undifferentiated colonies of human ESCs and iPSCs with αMEM supplemented with 20% FBS (SAFC Biosciences) and 0.1 mM β-mercaptoethanol in bacterial Petri dishes to form embryoid bodies. We observed embryoid bodies containing rhythmically beating cells 16–20 d later. Typically, 1–5% of embryoid bodies contained beating cells. From days 20 to 40, embryoid bodies were washed three times with αMEM and cultured with αMEM supplemented with ITS. Embryoid bodies were used for purification experiments between days 50 and 90.

Staining of cultured embryos. We isolated E11.5 and E12.5 Wistar rat embryos and stained with 50 nM TMRM for 4 h in DMEM with 20% FBS at 30% O_2, 5% CO_2 and 37 °C. Then, we changed to medium without TMRM and incubated the embryos for 4 h to remove unbound dye. We observed the fluorescence signal using conventional fluorescence laser microscopy (IX70 microscope (Olympus) equipped with a color charge-coupled device (CCD) camera (CS220; Olympus)).

Staining *in vivo* embryos. We carried out abdominal surgery on the pregnant Wistar rat on postcoital day 11 under deep anesthesia. We carried out a shallow injection of 100 μl of 500 nM MitoTracker Red solution into the placental side of the exposed ovaries. The rat was sustained under anesthesia for 6 h. Then, under deep anesthesia, we removed the embryos from the rat and observed them using fluorescence microscopy. About 20% of the embryos were positive for MitoTracker Red.

Cardiomyocyte purification. We dispersed the minced hearts, whole rat embryos, or intact embryoid bodies using 0.1% collagenase (Worthington Biochemical), 0.25% trypsin (Becton Dickinson), 20 μg ml^{-1} DNase I (Sigma) and the appropriate

doi:10.1038/nmeth.1403

concentration of dyes (10 nM TMRM, 50 nM NAO, 1.5 μM JC-1 or 50 nM MitoTrackers) in Ads buffer (116 mM NaCl, 20 mM HEPES, 12.5 mM NaH_2PO_4, 5.6 mM glucose, 5.4 mM KCl and 0.8 mM $MgSO_4$; pH 7.35) with stirring for 30 min. The dispersed cells were collected and residual cell aggregates were digested again with the same digestion medium. We continued this procedure until all cells were completely dissociated. Finally, all dispersed cells were dissociated with Ads buffer and then analyzed on a FACS (FACS Aria; Becton Dickinson) using 515–545 and 556–601 nm bandpass filters to detect green and red, respectively.

In many cases, nonstained cells exhibited autofluorescence, which may be due to the presence of lipopigments and flavins having broad emission spectrum (450–650 nm)[13]. We suspected that this may affect purity of cardiomyocytes. TMRM can be excited by a 488-nm semiconductor laser and has an emission spectrum that coincides with the red bandpass filter (peak at 575 nm and only 10% of peak fluorescence at 545 nm). Thus, to obtain only cells with high TMRM fluorescence and eliminate contaminating autofluorescent cells, we adopted 'pseudo–two-dimensional separation' in which we observed cells both with red and green filters. In other words, cardiomyocytes received 488 excitation, and then selection for low green and high red fluorescence. Pregating for eliminating doublet fractions, in which one droplet contains more than two cells, was performed according to the manufacturer's instructions.

The TMRM-labeled sorted cells were collected into a tube or were seeded into culture dishes with αMEM containing 10% FBS. For sequential estimation of cardiomyocyte purity, we fixed the sorted cells immediately after collection, then stained them with Nkx2.5 antibody and analyzed again on a FACS. For culture, we used a plate equipped with flexiPERM conA (Greiner Bio-One GmbH) following the manufacturer's instructions. The flexiPERM vessel is a reusable culture funnel, which can adhere tightly onto plastic and glass surfaces. One day after sorting, the flexiPERM vessel was detached from the culture plate and the appropriate amount of medium was added to the plate. This system allowed high-density culture of purified cardiomyocytes in the center of the dish, which enabled good microscopic observation of all cells after detachment of the vessel. For all PSCs, seeded cells were cultured for 5–7 d with αMEM containing 10% FBS, which is necessary for the cells to attach, elongate and develop sarcomere structure, and then fixed and immunofluorescence-stained for α-actinin and Nkx2.5. The culture step is not required for achieving high-purity cardiomyocyte isolation because we have more directly estimated cardiomyocyte purity by sequential FACS analysis.

Transplantation. We purified mouse and human ESC–derived cardiomyocytes, distributed them into nonadhesive 96-well plates (Sumitomo Bakelite) and centrifuged them for 5 min at 100*g*. Two weeks later, the aggregates formed were stained with 50 μM of MitoTracker Red for 2 h in the incubator and washed extensively with Ads buffer. After lightly anesthetizing seven-week-old male NOD-SCID mice with diethylether (Wako Pure Chemical), we intubated them under anesthetization with 1.5% forane (isoflurane, 2-chloro-2-(difluoromethoxy)-1,1,1-trifluoro-ethane) and mechanically ventilated with a Harvard respirator. After this, we performed a left thoracotomy at the third intercostal space and exposed the heart. We inserted a small dead-volume syringe equipped with a 30G needle (Becton Dickinson) containing reaggregated purified cardiomyocytes into the apex, proximally advanced 2–3 mm into the myocardium and released the cells into the myocardium. Then we closed the chest and maintained the mice for 8 weeks before performing a histological examination of these mice.

The 3-(4,5-dimethyl-thiazol-2-yl)-2,5-diphenyltetrazolium bromide (MTT) assay. We treated primary neonatal rat cardiomyocytes with various mitochondrial indicators at 50 nM and 100 nM for 24 h. We added MTT (Wako Pure Chemical) at 0.5 mg ml^{-1} and incubated the cardiomyocytes for 3 h. Then, we dissolved the formazan salt that formed in dimethyl sulfoxide. The absorbance was measured at a wavelength of 550 nm with the background subtracted at 690 nm (SmartSpec3000; Bio-Rad Laboratories). Data were presented as percentage of formazan formation compared to control cells.

Immunofluorescence staining. We fixed cells with 4% paraformaldehyde in phosphate-buffered saline (PBS; pH 7.0) for 20 min. Subsequently, cells were permeabilized with 0.2% Triton X-100 (Sigma) at room temperature (20–28 °C) for 10 min, and then incubated with the primary antibody at 4 °C overnight. Cells were washed with TBS containing 0.1% Tween-20 four times before incubation with the secondary antibodies at room temperature for 30 min. After nuclear staining with DAPI or ToPro-3 (Invitrogen), fluorescence signals were observed using fluorescence microscopy (IX71; Olympus) or confocal laser microscopy (LSM510 META; Carl Zeiss), respectively.

For tissue samples, mice were killed using pentobarbital. The hearts were then perfused from the apex with PBS and fixed by perfusion with 4% paraformaldehyde in PBS (Muto Pure Chemicals). The hearts were then dissected, cryoprotected in sucrose at 4 °C overnight, embedded in OCT compound (Sakura Finetec) and snap-frozen in liquid nitrogen.

Re-aggregation of purified human ESC–derived cardiomyocytes and long-term culture without serum. Human ESC–derived cardiomyocytes were purified and suspended in αMEM supplemented with insulin, transferrin and selenium (ITS) and 0.05% BSA (Invitrogen) in the absence or presence of one of the following growth factors: 25 ng ml^{-1} bFGF (Wako Pure Chemicals); 25 ng ml^{-1} acidic FGF (aFGF); 25 ng ml^{-1} FGF-4; 20 ng ml^{-1} keratinocyte growth factor (KGF); 100 ng ml^{-1} stem cell factor (SCF); 100 ng ml^{-1} vascular endothelial growth factor (VEGF); 10 ng ml^{-1} LIF (Chemicon); 100 ng ml^{-1} glial cell line–derived neurotrophic factor (GDNF); 20 ng ml^{-1} hepatocyte growth factor (HGF); 10 ng ml^{-1} insulin-like growth factor (IGF)-1; 100 ng ml^{-1} epidermal growth factor (EGF); 1×10^{7} M endothelin-1 (ET-1); 10 ng ml^{-1} platelet-derived growth factor (PDGF)-AA; and 100 ng ml^{-1} PDGF-BB. Unless indicated otherwise, growth factors were purchased from R&D Systems Inc. Five hundred cells were distributed into each well ($n = 8$) of cell nonadhesive 96-well plates (MS-0096S; Sumitomo Bakelite) and centrifuged for 5 min at 100*g*.

Total RNA extraction, cDNA synthesis and real-time PCR. Total RNA was prepared from tissues and embryoid bodies using ISOGEN (Nippon gene), according to the manufacturer's instructions. Contaminating genomic DNA was degraded by RNase-free DNase I

doi:10.1038/nmeth.1403

(Ambion) at 37 °C for 30 min. After treatment, DNase I was inactivated by phenol-chloroform extraction and ethanol precipitation. Human heart–derived total RNA was purchased from Takara Bio. We reverse transcribed total RNAs into cDNA using the oligo-(dT)12-18 primer (Superscript II RT kit; Invitrogen). We analyzed the mRNA expression on an ABI 7700 (Applied Biosystems). We listed the target gene name and identification numbers of the primer and probe mixtures (Applied Biosystems) in **Supplementary Table 1.**

21. Jakobs, S. High resolution imaging of live mitochondria. *Biochim. Biophys. Acta.* **1763**, 561–575 (2006).

doi:10.1038/nmeth.1403

Circulation Research

JOURNAL OF THE AMERICAN HEART ASSOCIATION

American Heart Association®

Learn and Live℠

The Cellular Prion Protein Identifies Bipotential Cardiomyogenic Progenitors

Kyoko Hidaka, Manabu Shirai, Jong-Kook Lee, Takanari Wakayama, Itsuo Kodama, Michael D. Schneider and Takayuki Morisaki

Circ. Res. 2010;106;111-119; originally published online Nov 12, 2009;
DOI: 10.1161/CIRCRESAHA.109.209478
Circulation Research is published by the American Heart Association. 7272 Greenville Avenue, Dallas, TX 72514
 Print ISSN: 0009-7330. Online ISSN: 1524-4571

The Cellular Prion Protein Identifies Bipotential Cardiomyogenic Progenitors

Kyoko Hidaka, Manabu Shirai, Jong-Kook Lee, Takanari Wakayama, Itsuo Kodama, Michael D. Schneider, Takayuki Morisaki

Rationale: The paucity of specific surface markers for cardiomyocytes and their progenitors has impeded the development of embryonic or pluripotent stem cell–based transplantation therapy. Identification of relevant surface markers may also enhance our understanding of the mechanisms underlying differentiation.

Objective: Here, we show that cellular prion protein (PrP) serves as an effective surface marker for isolating nascent cardiomyocytes as well as cardiomyogenic progenitors.

Methods and Results: Embryonic stem (or embryo-derived) cells were analyzed using flow cytometry to detect surface expression of PrP and intracellular myosin heavy chain (Myhc) proteins. Sorted cells were then analyzed for their differentiation potential.

Conclusions: PrP^+ cells from beating embryoid bodies (EBs) frequently included nascent $Myhc^+$ cardiomyocytes. Cultured PrP^+ cells further differentiated, giving rise to cardiac troponin I^+ definitive cardiomyocytes with either an atrial or a ventricular identity. These cells were electrophysiologically functional and able to survive in vivo after transplantation. Combining PrP with a second marker, platelet-derived growth factor receptor (PDGFR)α, enabled us to identify an earlier cardiomyogenic population from prebeating EBs, the $PrP^+PDGFR\alpha^+$ (PRa) cells. The $Myhc^-$ PRa cells expressed cardiac transcription factors, such as Nkx2.5, T-box transcription factor 5, and Isl1 (islet LIM homeobox 1), although they were not completely committed. In mouse embryos, PRa cells in cardiac crescent at the 1 to 2 somite stage were $Myhc^+$, whereas they were $Myhc^-$ at headfold stages. PRa cells clonally expanded in methlycellulose cultures. Furthermore, single $Myhc^-$ PRa cell–derived colonies contained both cardiac and smooth muscle cells. Thus, PrP demarcates a population of bipotential cardiomyogenic progenitor cells that can differentiate into cardiac or smooth muscle cells. (*Circ Res.* 2010;106:111-119.)

Key Words: cardiogenic precursor ■ differentiation ■ embryonic stem cells ■ surface marker regeneration

Heart, the first functional organ to develop in vertebrate embryos, contains cardiac, smooth muscle, and endothelial cells.[1–3] Cardiac transcription factors, such as Nkx2.5 (NK2 transcription factor related, locus 5) and T-box transcription factor (Tbx)5, are first expressed in cardiogenic mesoderm, which is located in the anterior lateral plate mesoderm.[4] Subsequently, genes encoding cardiac-specific structural proteins are expressed in the cardiac crescent.[4] The cardiac crescent then fuses at the ventral midline to form the linear heart tube, which develops into the chambered heart after looping. In the cardiac crescent, endothelial (or endocardial) markers, such as Flk1 (fetal liver kinase-1), do not markedly overlap with cardiomyogenic markers, suggesting that these 2 lineages have already segregated at this stage. Recent studies using embryonic stem (ES) cells have suggested the presence of multipotential cardiovascular stem cells that can differentiate into cardiac, smooth muscle, and endothelial cells[5,6]; these cells have been identified as $Flk1^+$ and/or islet LIM homeobox 1 $(Isl1)^+$.[7] Intermediate cardiomyogenic progenitor cells may be bipotential, differentiating into both cardiac and smooth muscle cells.[8] Because of the paucity of known specific surface markers, however, these intermediate progenitors have been difficult to characterize. Several studies using ES cells or embryonal carcinoma cells have suggested that temporally regulated Wnt signaling is important for the specification and differentiation of cardiomyocytes.[9–12] Progeny derived from ES cells, however, are a mixture of different cell types, and additional analysis is needed to define the immediate progenitors of cardiomyocytes more precisely.

Original received January 29, 2009; resubmission received September 18, 2009; revised resubmission received October 30, 2009; accepted November 3, 2009.

From the Department of Bioscience (K.H., M.S., T.W., T.M.), National Cardiovascular Center Research Institute, Suita, Japan; Department of Circulation (J.-K.L., I.K.), Research Institute of Environmental Medicine, Nagoya University, Japan; Department of Molecular Pathophysiology (T.W., T.M.), Osaka University Graduate School of Pharmaceutical Sciences Suita, Japan; and National Heart and Lung Institute (M.D.S.), Imperial College, London, United Kingdom.

Correspondence to Takayuki Morisaki, Department of Bioscience, National Cardiovascular Center Research Institute, -7-1 Fujishirodai, Suita, Osaka 565-8565, Japan. E-mail morisaki@ri.ncvc.go.jp

 DOI: 10.1161/CIRCRESAHA.109.209478

Non-standard Abbreviations and Acronyms	
ANP	atrial natriuretic peptide
cTn	cardiac troponin
E	embryonic day
EB	embryoid body
ES	embryonic stem
Flk1	fetal liver kinase-1
GFP	green fluorescent protein
Isl1	islet LIM homeobox 1
MEC	methylcellulose
Myhc	myosin heavy chain
Mylc	myosin light chain
Nkx2.5	NK2 transcription factor related, locus 5
PDGFR	platelet-derived growth factor receptor
PrP	prion protein
SMA	smooth muscle actin
SMMyhc	smooth muscle myosin heavy chain
Tbx	T-box transcription factor

In addition to their utility in developmental studies, ES cells or induced pluripotent stem cells are a potential cellular source for cell transplantation therapy to treat damaged hearts. Several groups have shown that transplanted ES cell–derived cells can repair damaged heart tissue.[13,14] In most of the previous studies, however, the transplanted cells were not purified cardiomyocytes, and including undifferentiated ES cells was often tumorigenic. To improve the efficacy of ES cell–derived cardiomyocytes, cardiomyocytes or committed progenitors should be isolated. Moreover, because functional engraftment requires a large number of cells, scalable and reproducible preparation methods should be developed. To date, few surface markers that can be used to isolate cardiomyocytes have been reported.[15] This has hindered efforts to isolate pure cardiomyocytes.

During course of studies to identify cardiogenesis-associated genes in ES cells,[16,17] we found that that *Prnp*, which encodes cellular prion protein (PrP), was expressed in cardiomyocyte-rich embryoid bodies (EBs). In this study, we show that PrP can be used to separate the cardiomyogenic and noncardiomyogenic cellular fractions. Furthermore, we identified a bipotential, $PrP^+PDGFR\alpha^+$ cardiomyogenic population that was able to differentiate into either cardiac or smooth muscle cells depending on Wnt signaling and the culture conditions.

Methods

ht7 cells (derived from the CGR8 cell line; a kind gift from Dr H. Niwa, RIKEN Center for Developmental Biology, Kobe, Japan) and the derivative hcgp7 cell line (Nkx2.5 EGFP [enhanced green fluorescent protein] knock-in) were maintained and differentiated as described previously.[1] Briefly, we created hanging drops (500 cells/drop) of differentiation medium containing 10% fetal calf serum (FCS) and Glasgow Minimum Essential Medium (GMEM). On day 2 of differentiation, medium was added to the plates and the cells were cultured as floating embryoid bodies (EBs). To differentiate EB3 ES cells (derived from the E14tg2a cell line; a kind gift from Dr Niwa), Minimum Essential Medium Eagle Alpha Modification (αMEM) was used as the basal medium instead of GMEM. Typically, ht7 and hcgp7 cells began to beat spontaneously on day 7, whereas EB3 cells began beating on day 6. The percentages of beating EBs were approximately 100% (ht7 and hcgp7 cells) and 80% (EB3 cells).

An expanded Methods section is available in the Online Data Supplement at http://circres.ahajournals.org.

Results

PrP Is Expressed in ES Cell–Derived Cardiomyocytes

To confirm that *Prnp* was expressed in EBs during cardiogenesis, we performed RT-PCR analysis. *Prnp* expression was upregulated by 7- to 8-fold before spontaneous beating began (Online Figure I, A). In beating EBs, the PrP^+ area partially overlapped with the area containing sarcomeric tropomyosin protein–expressing cardiomyocytes (Online Figure I, B). Although the physiological functions of PrP are not yet known,[18] PrP has been detected on the surface membranes of various cell types.[19] To examine the specificity of PrP expression at the cellular level, we used flow cytometry to examine an ES cell line in which *EGFP* was knocked into the *Nkx2.5* locus ($Nkx2.5^{GFP/+}$ ES cells)[20]; all of the green fluorescent protein $(GFP)^+$ cardiomyocytes expressed PrP on their surfaces on day 7 (Figure 1A). Although GFP has been used to isolate cardiomyocytes from beating EBs, we

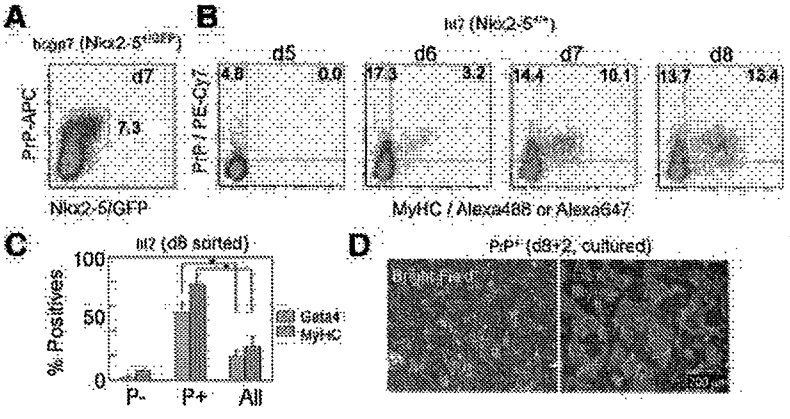

Figure 1. PrP is expressed in ES cell-derived cardiomyocytes. A, Flow cytometric analysis of PrP cell surface expression in $Nkx2.5^{GFP/+}$ ES cells (hcgp7). On day 7 of differentiation, GFP^+ cardiomyocytes were found in the PrP^+ fraction. B, Flow cytometric analysis of cell surface PrP and intracellular sarcomeric Myhc in the parental cell line of hcgp7 cells (ht7). After staining the cells with an anti-PrP antibody, the cells were fixed, permeabilized, and stained with an anti-Myhc antibody. The earliest $Myhc^+$ cells appeared on day 6 and were all PrP^+. C and D, Cardiomyocyte samples were enriched from beating EBs using the anti-PrP antibody. Cells were analyzed for Myhc and GATA-binding protein 4 (Gata4) expression immediately after cell sorting (C) or after they had been cultured on gelatin-coated plates for 2 days (D). Error bars represent the SEMs (n=3 independent samples for each group). $^*P<0.05$ from an unpaired Student *t* test.